LETTER

https://doi.org/10.1038/s41586-019-1215-2

Targeting the CBM complex causes T_{reg} cells to prime tumours for immune checkpoint therapy

Mauro Di Pilato[1,2,6]*, Edward Y. Kim[1,2,6], Bruno L. Cadilha[1], Jasper N. Prüßmann[1,2], Mazen N. Nasrallah[1,2], Davide Seruggia[2,3], Shariq M. Usmani[1,2], Sandra Misale[2,4], Valentina Zappulli[5], Esteban Carrizosa[1,2], Vinidhra Mani[1,2], Matteo Ligorio[2,4], Ross D. Warner[1], Benjamin D. Medoff[1,2], Francesco Marangoni[1,2], Alexandra-Chloe Villani[1,2] & Thorsten R. Mempel[1,2]*

Solid tumours are infiltrated by effector T cells with the potential to control or reject them, as well as by regulatory T (T_{reg}) cells that restrict the function of effector T cells and thereby promote tumour growth[1]. The anti-tumour activity of effector T cells can be therapeutically unleashed, and is now being exploited for the treatment of some forms of human cancer. However, weak tumour-associated inflammatory responses and the immune-suppressive function of T_{reg} cells remain major hurdles to broader effectiveness of tumour immunotherapy[2]. Here we show that, after disruption of the CARMA1–BCL10–MALT1 (CBM) signalosome complex, most tumour-infiltrating T_{reg} cells produce IFNγ, resulting in stunted tumour growth. Notably, genetic deletion of both or even just one allele of *CARMA1* (also known as *Card11*) in only a fraction of T_{reg} cells—which avoided systemic autoimmunity—was sufficient to produce this anti-tumour effect, showing that it is not the mere loss of suppressive function but the gain of effector activity by T_{reg} cells that initiates tumour control. The production of IFNγ by T_{reg} cells was accompanied by activation of macrophages and upregulation of class I molecules of the major histocompatibility complex on tumour cells. However, tumour cells also upregulated the expression of PD-L1, which indicates activation of adaptive immune resistance[3]. Consequently, blockade of PD-1 together with CARMA1 deletion caused rejection of tumours that otherwise do not respond to anti-PD-1 monotherapy. This effect was reproduced by pharmacological inhibition of the CBM protein MALT1. Our results demonstrate that partial disruption of the CBM complex and induction of IFNγ secretion in the preferentially self-reactive T_{reg} cell pool does not cause systemic autoimmunity but is sufficient to prime the tumour environment for successful immune checkpoint therapy.

Local exposure of tumour-infiltrating T_{reg} cells to their cognate antigens sustains their tumour-promoting immunosuppressive functions[4]. We therefore explored which T-cell-receptor (TCR)-dependent signalling pathways could be targeted to disable tumour-reactive T_{reg} cells. The scaffold protein CARMA1 nucleates assembly of the CBM complex in T cells in response to TCR-dependent PKCθ activity and promotes several functions, including activation of the AP-1, mTOR and classical NF-κB pathways, as well as stabilization of mRNA[5]. Constitutive genetic deletion of CARMA1, BCL10 or MALT1 abrogates thymic development of T_{reg} cells[6–10], but their role in mature T_{reg} cells is unknown.

When we conditionally deleted either one or both alleles of *CARMA1* in mature T_{reg} cells by crossing *Foxp3*$^{YFP\text{-}cre}$ to *CARMA1*$^{flox/flox}$ mice (hereafter referred to as $F^{cre} \times C1^{f/+}$ or $F^{cre} \times C1^{f/f}$ mice), levels of CARMA1 protein were proportionally reduced in $CD4^+FOXP3^+$ T_{reg} cells from lymph nodes (LNs) (Extended Data Fig. 1a). $F^{cre} \times C1^{f/f}$, but not $F^{cre} \times C1^{f/+}$ or $C1^{+/+}$ control mice, stopped thriving at 17 days; most died before 4 weeks of age after a T-helper-1 (T_H1)-dominated multiorgan inflammatory disease characterized by splenomegaly, lymphadenopathy, effector differentiation and inflammatory cytokine secretion by conventional T (T_{conv}) cells, production of autoreactive IgG, and activation of the myeloid compartment (Fig. 1a, Extended Data Figs. 1b–f, 2a–f). Hence, CARMA1 is essential for T_{reg} cells to maintain immune homeostasis, but a reduction in its expression at least up to 50% is tolerated.

Absolute numbers of T_{reg} cells were increased in LNs of $F^{cre} \times C1^{f/f}$ mice, concomitant with an increase in overall LN cellularity (Extended Data Fig. 2g, h). However, the overall frequency of T_{reg} cells among $CD4^+$ T cells did not vary with CARMA1 expression, whereas the proportion of $CD44^{high}CD62L^-$ effector T_{reg} (eT_{reg}) was strongly reduced in its absence (Fig. 1b). Notably, CARMA1-deficient T_{reg} cells, while retaining expression of FOXP3, almost uniformly secreted IFNγ and—at lower frequencies—secreted IL-4, IL-17 and TNF (Fig. 1c). Although nearly all CARMA1-deficient T_{reg} cells secreted the T_H1-cytokine IFNγ, far fewer—and only eT_{reg} cells—expressed the T_H1 lineage-defining transcription factor T-bet along with RORγt and, to a lesser degree, GATA-3 (Fig. 1d and Extended Data Fig. 2i, j). Hence, complete—but not partial—deletion of CARMA1 in T_{reg} cells markedly dysregulates their cytokine expression that (in the case of IFNγ) is dissociated from expression of T-bet, and may contribute to the pathogenesis of inflammatory disease. Indeed, $F^{cre} \times C1^{f/f}$ mice died more rapidly than T_{reg} cell-deficient *scurfy* mice, but their lifespans were similar when IFNγ was neutralized (Fig. 1e). Thus, under inflammatory conditions, CARMA1-deficient T_{reg} cells convert from an immunoregulatory cell type into an IFNγ-secreting pathogenic cell type.

In heterozygous female $F^{cre/+} \times C1^{f/f}$ mice, random inactivation of the X chromosome causes the yellow fluorescent protein–Cre recombinase (YFP–Cre) fusion protein to be expressed and CARMA1 to be deleted in only half of the T_{reg} cells, whereas the other half maintains immune homeostasis (Extended Data Fig. 3a–c). Under such non-inflammatory conditions, CARMA1-deficient T_{reg} cells did not secrete effector cytokines (Fig. 1f). However, in competition with CARMA1-sufficient T_{reg} cells for niche space, we observed a proportional decline specifically in the frequency of eT_{reg} cells—but not of central T_{reg} (cT_{reg}) cells—that lacked one or both alleles of *CARMA1* (Fig. 1g and Extended Data Fig. 3e). The remaining YFP^+ eT_{reg} cells expressed less FOXP3 and other proteins that are characteristically increased in expression during the differentiation of cT_{reg} cells into eT_{reg} cells (Fig. 1h). They expressed more of the pro-apoptotic protein BIM, but also more of the anti-apoptotic protein BCL2, which probably reflects impaired differentiation of eT_{reg} cells, as control eT_{reg} cells strongly downregulated both BCL2 and BIM relative to cT_{reg} cells (Extended Data Fig. 3d–h). The in vitro suppressive function of CARMA1-deficient T_{reg} cells was reduced, but not abrogated (Extended Data Fig. 4a, b), and they failed to persist and did not suppress lymphopenia-induced expansion of effector T cells after transfer into RAG1-deficient hosts (Extended Data Fig. 4c). Failure to persist in vivo did not seem to result from accelerated apoptosis, because the previously described high apoptotic rate of eT_{reg} cells[11]

[1]Center for Immunology and Inflammatory Diseases, Massachusetts General Hospital, Boston, MA, USA. [2]Harvard Medical School, Boston, MA, USA. [3]Division of Hematology/Oncology, Boston Children's Hospital, Boston, MA, USA. [4]Center for Cancer Research, Massachusetts General Hospital, Boston, MA, USA. [5]Department of Comparative Biomedicine and Food Science, University of Padua, Padova, Italy. [6]These authors contributed equally: Mauro Di Pilato, Edward Y. Kim. *e-mail: mdipilato@mgh.harvard.edu; tmempel@mgh.harvard.edu

was not further enhanced in the absence of CARMA1 (Extended Data Fig. 4d). Lack of CARMA1 did not lead to an increase in the formation of FOXP3-negative 'exT_{reg}' cells (Extended Data Fig. 4e).

On the basis of global gene expression analyses, CARMA1-deficient eT_{reg} cells were equally dissimilar to control eT_{reg} cells as they were to control cT_{reg} cells, whereas CARMA1-deficient cT_{reg} cells were only moderately dissimilar to control cT_{reg} cells (Fig. 1i). In the latter, only 96 genes were differentially expressed, compared with 344 genes in eT_{reg} cells (Extended Data Fig. 5a and Supplementary Table 1). Based on differences between control cT_{reg} and eT_{reg} cells, we defined an 'eT_{reg} signature', which largely overlapped with a previously reported gene set[12,13]. When examining these 689 genes, hemizygous *CARMA1*-deletion had only a moderate effect, whereas homozygous deletion induced major changes specifically in the eT_{reg} cell gene expression program (Fig. 1j and Extended Data Fig. 5b). Minor changes in the expression of the Bcl2 family of apoptotic regulator genes occurred during eT_{reg} cell differentiation, but CARMA1-deficient eT_{reg} cells did not deviate from this pattern apart from having less pronounced downregulation of BCL2 and BIM, confirming our observations on protein expression (Extended Data Fig. 6). Thus, a complete—and even a partial—loss of CARMA1 expression impairs eT_{reg} cell differentiation and persistence, but does not induce the cells to become pathogenic or convert to exT_{reg} cells under non-inflammatory conditions. However, in the context of incipient inflammation trigged by a global loss of the suppressive function of T_{reg} cells, CARMA1-deficient T_{reg} cells secrete IFNγ, which further accelerates inflammatory disease.

Failed thymic development of T_{reg} cells in the absence of CARMA1 results from disabled NF-κB signalling and is restored through the expression of a constitutively active form of IκB kinase 2 (referred to as IKK2ca)[12]. Furthermore, the NF-κB proteins REL (also known as c-Rel) and RELA (p65) have important roles in T_{reg} cell function[13–15], which suggests that failed activation of NF-κB may primarily account for the effects of CARMA1-deletion in T_{reg} cells. However, the expression of IKK2ca in T_{reg} cells neither prolonged the lifespan of $F^{cre} \times C1^{f/f}$ mice, nor reduced the differentiation of effector T_{conv} cells (Extended Data Fig. 7a, b). Restoring NF-κB activation did not restore differentiation of eT_{reg} cells, and did not limit the secretion of IFNγ, but only of TNF (Extended Data Fig. 7c, d). Therefore, although NF-κB activation is evidently essential[13,16], additional CBM-complex effector functions are also crucial for maintaining T_{reg} cell function. The relevance of these additional functions will need to be investigated, but an initial examination of CARMA1-deficient T_{reg} cells from healthy $F^{cre/+} \times C1^{f/f}$ mice already revealed decreased expression and TCR-induced phosphorylation of the AP-1 family protein JUN, as well as changes to phosphorylation of FOXO1, possibly reflecting CARMA1- and TBK1-driven regulation of AKT activity[17] (Extended Data Fig. 7e, f).

Considering the pro-inflammatory potential of CARMA1-deficient T_{reg} cells, we examined their tumour response. Subcutaneous implantation of the poorly immunogenic $Braf^{V600E} \times Pten^{-/-}$ melanoma D4M.3A[18] into female $F^{cre/+} \times C1^{f/f}$ hosts amplified the effects of CARMA1-deficiency on T_{reg} cells, because the frequency not only of eT_{reg} cells but also of total T_{reg} cells was reduced in tumours and tumour-draining LNs (tdLNs) as a function of decreasing CARMA1 expression, accompanied also by a more pronounced reduction in FOXP3 expression (Extended Data Fig. 8a–d). Notably, we observed growth deceleration of D4M.3A melanoma, and of MC38 colon carcinoma, when half of the T_{reg} cells lacked one or both alleles of *CARMA1* (Fig. 2a and Extended Data Fig. 8e). Because a mere loss of function in only half of the T_{reg} cells is not predicted to cause loss of tumour tolerance[19], this suggested active T_{reg}-cell-mediated anti-tumour activity. Indeed, a large fraction of completely or even partially CARMA1-deficient T_{reg} cells secreted both TNF and IFNγ in situ, whereas these effector cytokines were undetectable in tumour-infiltrating $CD4^+$ and $CD8^+$ T_{conv} cells (Fig. 2b, c). Importantly, no increase in cytokine secretion by T_{reg} cells was observed in tdLNs or in non-lymphoid tissues, such as skin or lung (Fig. 2d and Extended Data Fig. 8f, g). IFNγ expression in tumour tissue correlated with downregulation, but not

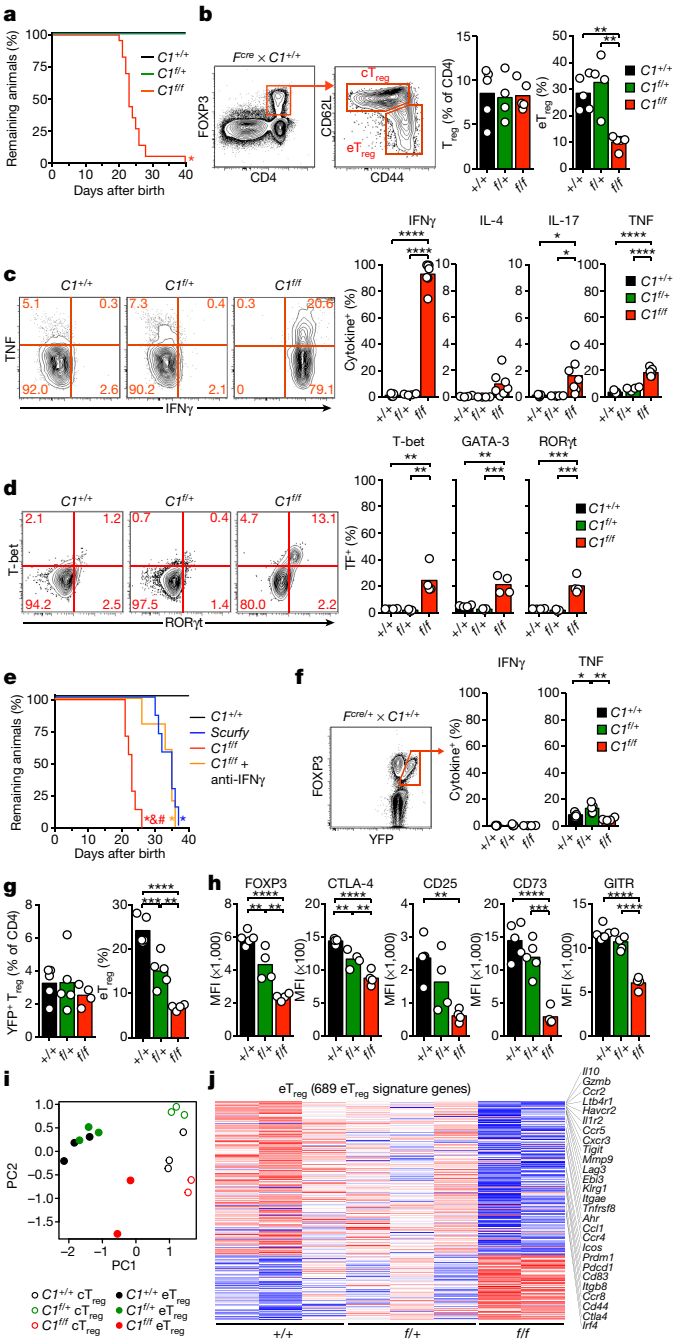

Fig. 1 | Loss of CARMA1 in T_{reg} cells is fatal, but reduced expression is sufficient to maintain immune tolerance. a, Survival of $F^{cre} \times C1^{+/+}$, $C1^{f/+}$ and $C1^{f/f}$ mice ($n = 8$, 10 and 20 per group, respectively). **b**, Frequency of T_{reg} cells among $CD4^+$ T cells and of eT_{reg} cells among total T_{reg} cells in LNs. **c**, **d**, Expression of cytokines (**c**) and transcription factors (TF) (**d**) in LN T_{reg} cells after ex vivo stimulation. **e**, Survival of $F^{cre} \times C1^{f/f}$ mice treated with anti-IFNγ antibodies from day 14 of life, compared with $F^{cre} \times C1^{+/+}$ and *scurfy* mice. **f**, Cytokine expression of YFP^+ T_{reg} cells from LNs of nine-week-old female heterozygous $F^{cre/+} \times C1^{+/+}$, $C1^{f/+}$ and $C1^{f/f}$ mice after ex vivo stimulation. **g**, Frequency of YFP^+ T_{reg} cells among $CD4^+$ T cells and of YFP^+ eT_{reg} cells among total YFP^+ T_{reg} cells in LNs. **h**, Expression of indicated proteins in YFP^+ eT_{reg} cells from 9-week-old mice. Data in **b**–**h** represent two independent experiments with similar results. Data are mean and individual replicates. In **a** and **e**, $^*P < 0.05$ versus wild type (+/+), $\&P < 0.05$ versus *scurfy*, and $\#P < 0.05$ versus anti-IFNγ (log-rank (Mantel–Cox) test). In all other panels, $^*P < 0.05$, $^{**}P < 0.01$, $^{***}P < 0.001$, $^{****}P < 0.0001$ (one-way analysis of variance (ANOVA) with Tukey post hoc test). **i**, **j**, Bulk RNA sequencing analysis of YFP^+ cT_{reg} and eT_{reg} cells from LNs of $F^{cre/+} \times C1^{+/+}$, $C1^{f/+}$ and $C1^{f/f}$ mice. **i**, Principal component (PC) analysis of transcriptomes. **j**, Scaled expression of eT_{reg} signature genes by eT_{reg} cells (defined by fold change > 2 and $P_{adj} < 0.01$ between $C1^{+/+}$ cT_{reg} and $C1^{+/+}$ eT_{reg} cells). Selected eT_{reg} cell genes are annotated.

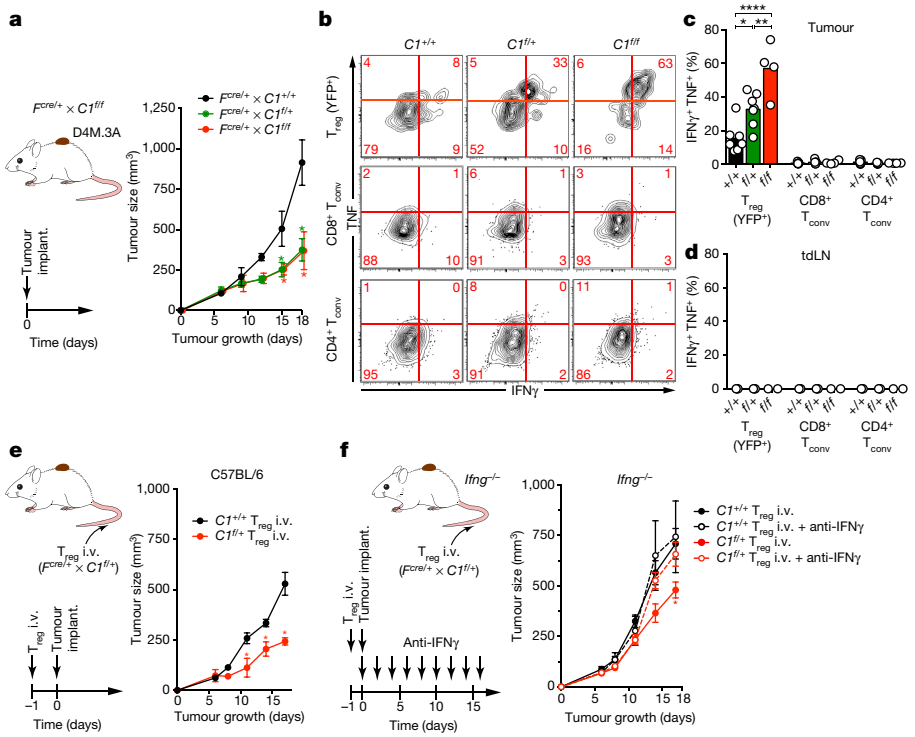

Fig. 2 | Reduced CARMA1 expression converts tumour-infiltrating T_{reg} cells into IFNγ-secreting effector cells that dominantly control tumour growth. a, Female $F^{cre/+} \times C1^{+/+}$, $C1^{f/+}$ and $C1^{f/f}$ mice were implanted with D4M.3A melanoma, and tumour growth was recorded. **b**–**d**, In situ expression in tumour tissue (**b**, **c**) or tdLNs (**d**) of effector cytokines in YFP^+ T_{reg} cells lacking one or both alleles of *CARMA1* as well as in $CD4^+$ and $CD8^+$ T_{conv} cells 18 days after tumour implantation. **e**, **f**, One million YFP^+ T_{reg} cells from $F^{cre/+} \times C1^{f/+}$ or $C1^{+/+}$ mice were injected intravenously (i.v.) into either C57BL/6 (**e**) or IFNγ-deficient (**f**) hosts, which were implanted with D4M.3A melanoma the next day, and tumour growth was recorded. Some IFNγ-deficient hosts were treated with neutralizing anti-IFNγ antibody. Data represent two independent replicates with similar results. Data are mean and either individual replicates (**c**, **d**) or s.e.m. (**a**, **e**, **f**). $^*P < 0.05$, $^{**}P < 0.01$, $^{****}P < 0.0001$ (two-way ANOVA with Bonferroni post hoc test in **a**, **f**; one-way ANOVA with Tukey post hoc test in **c**, **d**; two-tailed Student's *t*-test in **e**).

loss of FOXP3 in both partially and fully CARMA1-deficient T_{reg} cells (Extended Data Fig. 8h). Notably, destabilization of control T_{reg} cells by IFNγ-producing T_{reg} cells, as described in other settings[20], did not occur because no increase in cytokine expression was detectable in YFP^- CARMA1-sufficient T_{reg} cells in the same tumours (not shown). Neutralization of IFNγ fully restored tumour growth in $F^{cre/+} \times C1^{f/f}$ mice (Extended Data Fig. 8i), which suggests a crucial role for this cytokine in T_{reg}-cell-mediated anti-tumour immunity. However, IFNγ may also derive from other cellular sources after T_{reg} cell destabilization. To test the role of T_{reg}-cell-produced IFNγ specifically, we transferred T_{reg} cells with reduced expression of CARMA1 into tumour-bearing $C57BL/6$ or $Ifng^{-/-}$ mice. In both hosts, T_{reg} cells stunted tumour growth similarly, but not when IFNγ was neutralized, which indicates that T_{reg}-cell-derived IFNγ is both necessary and sufficient for anti-tumour effects (Fig. 2e, f and Extended Data Fig. 8j–m). Therefore, although neither partially nor fully CARMA1-deficient T_{reg} cells cause inflammation in healthy mice, both are selectively destabilized in tumour tissue and secrete IFNγ to decelerate tumour growth.

Expression of IKK2ca restored the frequencies of total T_{reg} and eT_{reg} cells in tdLNs, but not in tumour tissue (Extended Data Fig. 9a). It did not restore FOXP3 expression, only partially reduced TNF and IFNγ co-expression by tumour-infiltrating CARMA1-deficient

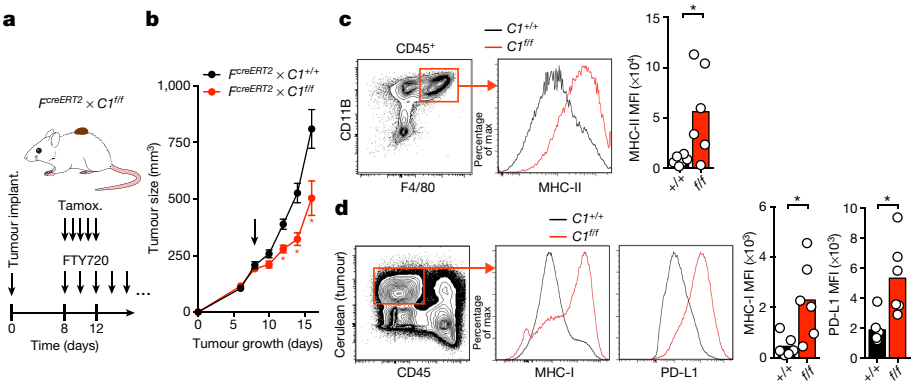

Fig. 3 | CARMA1-deleted T_{reg} cells rapidly induce tumour inflammation but also adaptive immune resistance. a, **b**, D4M.3A melanoma growth in $F^{creERT2} \times C1^{+/+}$ and $C1^{f/f}$ mice treated with tamoxifen from days 8–12 as well as with FTY720 starting the same day until the end of the experiment. Arrow in **b** indicates the start of treatment. **c**, **d**, MHC-II surface expression on $F4/80^+$ tumour macrophages (**c**), and MHC-I and PD-L1 expression on D4M.3A tumour cells (expressing blue-fluorescent H2B-Cerulean) (**d**) three days after the initiation of tamoxifen treatment. MFI, mean fluorescence intensity. Data represent two independent replicates with similar results. Data are mean and individual replicates (**c**, **d**) or s.e.m. (**b**). $^*P < 0.05$ (two-tailed Student's *t*-test).

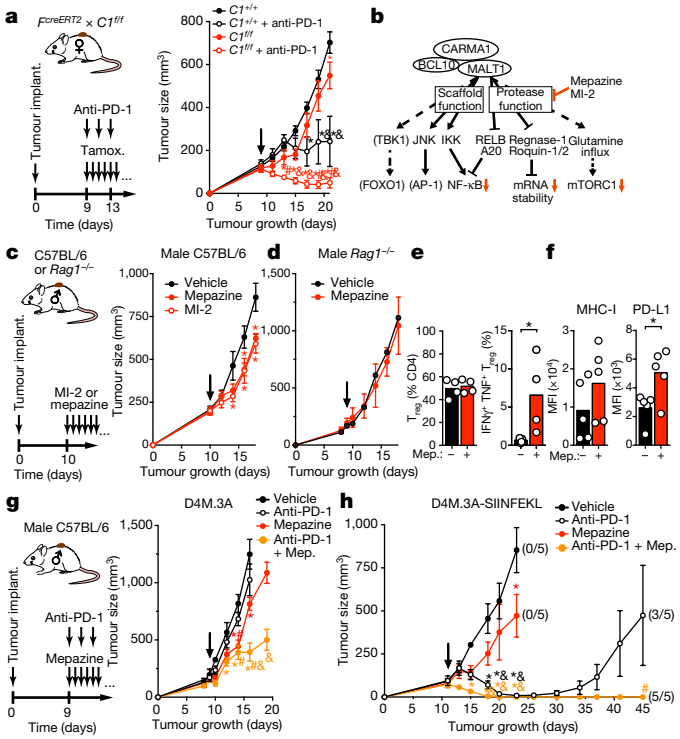

Fig. 4 | CARMA1 deletion in T_{reg} cells and pharmacological inhibition of MALT1 protease synergize with anti-PD-1 ICT. a, Female $F^{creERT2} \times C1^{+/+}$ and $C1^{f/f}$ mice were implanted with D4M.3A melanoma, and treated with tamoxifen starting on day 9 until the end of the experiment, as well as with three doses of the anti-PD-1-antibody 29F.1A12 or isotype control, and tumour growth was recorded. **b**, CBM complex effector pathways and predicted effects (red arrows) of the MALT1 protease inhibitors mepazine and MI-2. **c**, **d**, D4M.3A tumour growth in C57BL/6 (**c**) or RAG1-deficient (**d**) hosts treated with MALT1 inhibitors (MI-2 or mepazine). Dimethylsulfoxide (DMSO) was used as a vehicle control. **e**, **f**, Effects of mepazine treatment for three days on intratumoral T_{reg} cell frequency and their in situ expression of effector cytokines (**e**), and on the expression of MHC-I and PD-L1 on tumour cells (**f**). **g**, **h**, Synergistic control of tumours by combined anti-PD-1 and mepazine treatment of poorly immunogenic D4M.3A (**g**) and immunogenic D4M.3A-SIINFEKL (**h**) tumours in male C57BL/6 hosts. Numbers in parentheses indicate fraction of mice without relapse for more than 12 months after discontinuation of treatment. Data in **a**, **c**–**f** represent two independent replicates with similar results. Data are mean and individual replicates (**e**, **f**) or s.e.m. (**a**, **c**, **d**, **g**, **h**). Arrows in tumour growth charts indicate the start of treatment. In **a**, $*P < 0.05$ versus $C1^{+/+}$, $\#P < 0.05$ versus $C1^{+/+}$ + anti-PD-1, and $\&P < 0.05$ versus $C1^{f/f}$. In **g** and **h**, $*P < 0.05$ versus vehicle (DMSO), $\#P < 0.05$ versus anti-PD-1, and $\&P < 0.05$ versus and mepazine, respectively. In **e**, $*P < 0.05$ (two-way ANOVA with Bonferroni post hoc test in **a**, **c**, **g**, **h**; two-tailed Student's *t*-test in **d**–**f**).

T_{reg} cells, and did not prevent their anti-tumour activity (Extended Data Fig. 9b–d), which emphasizes the importance of CBM-complex effector functions other than NF-κB activation[16] in stabilizing tumour-reactive T_{reg} cells.

To examine whether CARMA1 deletion acutely destabilizes intratumoral T_{reg} cells, we generated $Foxp3^{GFP\text{-}creERT2} \times CARMA1^{f/f}$ (hereafter termed $F^{creERT2} \times C1^{f/f}$) mice and treated these with tamoxifen to trigger Cre-mediated CARMA1 deletion when tumours were already established (Fig. 3a and Extended Data Fig. 9e). To prevent subsequent recruitment of additional T_{reg} cells from tdLNs, we concurrently blocked lymphocyte tissue egress using the functional S1P receptor antagonist FTY720, as previously described[4]. Within two days of treatment, tumour growth decelerated (Fig. 3b). A similarly rapid, albeit slightly less pronounced, growth effect as well as increased secretion of effector cytokines by T_{reg} cells resulted from deletion of CARMA1 in only half of the T_{reg} cells (Extended Data Fig. 9f, g). Intratumoral destabilization of T_{reg} cells was accompanied by pronounced induction of macrophage expression of cell-surface major histocompatibility complex class II (MHC-II) molecules, both after constitutive or acute deletion of one or both alleles of *CARMA1* in T_{reg} cells (Fig. 3c and Extended Data Fig. 9h). Furthermore, the expression of MHC-I molecules on tumour cells increased, predictably sensitizing them to cytotoxic-T-lymphocyte (CTL)-mediated lysis (Fig. 3d). Although T_{reg} cell-derived IFNγ thus caused widespread tumour inflammation, it also triggered tumour cell-expression of PD-L1, a ligand for the T cell inhibitory receptor PD-1, which suggests that concurrent induction of adaptive immune resistance[3] limited improved tumour control resulting from enhanced anti-tumour immune effector functions (Fig. 3d).

Considering the induction of PD-L1 on tumour cells, we hypothesized that antibody-mediated blockade of PD-1 may synergize with the anti-tumour effects of IFNγ-secreting T_{reg} cells. Indeed, treatment with anti-PD-1 antibody simultaneously with CARMA1 deletion in T_{reg} cells enabled much more rapid and consistent control of D4M.3A melanoma than either treatment alone (Fig. 4a). Targeting the CBM complex in T_{reg} cells may thus be highly effective at enhancing the potency of immune checkpoint therapy (ICT) in patients with cancer.

Although pharmacological inhibitors of the scaffold protein CARMA1 are, to our knowledge, currently not available, inhibitors of MALT1 paracaspase are predicted to attenuate the majority of CBM-complex-dependent effector pathways (Fig. 4b). Indeed, similar to CARMA1-deficient mice, T_{reg} cells are virtually absent in mice that express mutant MALT1 proteins that lack paracaspase activity (replicating continual and complete pharmacological inhibition)[21–23]. We therefore tested the allosteric MALT1 inhibitor mepazine[24,25] and the catalytic site binder MI-2[26] for activity against solid tumours. Both inhibitors produced a similar deceleration in melanoma growth to that observed after deletion of CARMA1 in T_{reg} cells (Fig. 4c), even when $CD8^+$ T cells were depleted (Extended Data Fig. 9i). Systemic inhibition of MALT1 will also target cells other than T_{reg} cells, including melanoma cells[27]. However, no effect on tumour growth occurred in RAG1-deficient mice that lack lymphocytes (Fig. 4d). Inhibition of MALT1 did not synergize with deletion of CARMA1 in T_{reg} cells, which suggests that the anti-tumour activity of MALT1 does not result from effects other than attenuated CBM complex function in T_{reg} cells (Extended Data Fig. 9j). Because MALT1 inhibition is predicted to attenuate, and not enhance lymphocyte effector functions[28], we conclude that its effect on tumour growth is probably mediated through destabilization of T_{reg} cells. Similar to T_{reg}-cell-specific deletion of CARMA1, treatment with mepazine caused a rapid, albeit less pronounced, induction of TNF and IFNγ expression by tumour-infiltrating T_{reg} cells (Fig. 4e). Short-term in vitro treatment of T_{reg} cells triggered only a minor reduction of FOXP3, GITR and CTLA-4 expression (Extended Data Fig. 10a) and did not induce IFNγ secretion (data not shown), which indicates that the latter occurs only under the conditions of the tumour microenvironment. Accordingly, mepazine caused upregulation of the expression of PD-L1 and MHC-I molecules on tumour cells in vivo (Fig. 4f) and induction of *Ifng* and a wide range of IFNγ-regulated genes indicative of both T_H1 inflammation and adaptive immune resistance in tumour tissue (Extended Data Fig. 10b). In contrast to constitutive deletion of CARMA1, short-term inhibition of MALT1 did not reduce the frequency of T_{reg} cells, and the expression of T_{reg}-cell-associated genes in tumour tissue was not reduced (Fig. 4e and Extended Data Fig. 10c). Nevertheless, in addition to overall enhanced infiltration of immune cells, treatment with mepazine specifically increased the frequencies of CTL and natural killer cells in tumour tissue (Extended Data Fig. 10d–h).

A high tumour mutational load favours response to ICT in patients with cancer[29,30], and a low mutational burden remains a major challenge that limits the success of this form of immunotherapy to some cancer types and to a minority of patients. Accordingly, D4M.3A melanoma, which carries a negligible mutational load relative to the C57BL/6J reference exome (D. E. Fisher, personal communication),

is completely resistant to anti-PD-1 monotherapy in male hosts (Fig. 4g), in contrast to female hosts, in which Y-antigen-expressing male D4M.3A tumours showed a partial response (Fig. 4a). Concurrent MALT1 inhibition, however, synergized with anti-PD-1 treatment, and arrested tumour growth even in male hosts (Fig. 4g). Anti-PD-1 treatment did not further increase T_{reg} cell expression of IFNγ, indicating that PD-1 did not restrict the pro-inflammatory function of destabilized T_{reg} cells (Extended Data Fig. 10i). Furthermore, when we raised the immunogenicity of D4M.3A tumours by expressing the chicken ovalbumin-derived SIINFEKL epitope as a surrogate mutational neoantigen, we observed an initial response to anti-PD-1 monotherapy, but 40% of tumours relapsed. A combination of anti-PD-1 antibodies with mepazine, however, produced accelerated rejection and prevented relapse (Fig. 4h). Finally, to explore the effects of MALT1 inhibition on other cancer types, we treated mice implanted with MC38 colon carcinoma. Although anti-PD-1 monotherapy had only a moderate effect on late-stage tumours, combination with mepazine enabled profound tumour control and relapse-free rejection in most mice (Extended Data Fig. 10j). Hence, systemic inhibition of MALT1 inflames the tumour environment and renders poorly immunogenic tumours responsive to anti-PD-1 therapy while enhancing responses of immunogenic tumours and minimizing the frequency of relapse, a common problem in clinical ICT[31].

We propose that inhibition of MALT1 protease or of other CBM complex functions could be a useful therapeutic strategy to elicit an intratumoral T_H1 autoimmune reaction mediated by locally destabilized, preferentially self-reactive T_{reg} cells. Pro-inflammatory effects of destabilized T_{reg} cells seem to outweigh any potential attenuation of immune effector cell activities through MALT1 inhibition. Owing to its selectivity for intratumoral T_{reg} cells, this treatment may increase the fraction of patients with cancer who respond to PD-1/PD-L1-targeted ICT or other forms of immunotherapy, without inducing systemic autoimmune toxicity.

Online content

Any methods, additional references, Nature Research reporting summaries, source data, statements of data availability and associated accession codes are available at https://doi.org/10.1038/s41586-019-1215-2.

Received: 15 December 2017; Accepted: 17 April 2019;
Published online 15 May 2019.

1. Savage, P. A., Leventhal, D. S. & Malchow, S. Shaping the repertoire of tumor-infiltrating effector and regulatory T cells. *Immunol. Rev.* **259**, 245–258 (2014).
2. Mellman, I., Coukos, G. & Dranoff, G. Cancer immunotherapy comes of age. *Nature* **480**, 480–489 (2011).
3. Spranger, S. et al. Up-regulation of PD-L1, IDO, and T_{regs} in the melanoma tumor microenvironment is driven by $CD8^+$ T cells. *Sci. Transl. Med.* **5**, 200ra116 (2013).
4. Bauer, C. A. et al. Dynamic T_{reg} interactions with intratumoral APCs promote local CTL dysfunction. *J. Clin. Invest.* **124**, 2425–2440 (2014).
5. Meininger, I. & Krappmann, D. Lymphocyte signaling and activation by the CARMA1-BCL10-MALT1 signalosome. *Biol. Chem.* **397**, 1315–1333 (2016).
6. Medoff, B. D. et al. Differential requirement for CARMA1 in agonist-selected T-cell development. *Eur. J. Immunol.* **39**, 78–84 (2009).
7. Molinero, L. L. et al. CARMA1 controls an early checkpoint in the thymic development of $FoxP3^+$ regulatory T cells. *J. Immunol.* **182**, 6736–6743 (2009).
8. Barnes, M. J. et al. Commitment to the regulatory T cell lineage requires CARMA1 in the thymus but not in the periphery. *PLoS Biol.* **7**, e1000051 (2009).
9. Brüstle, A. et al. MALT1 is an intrinsic regulator of regulatory T cells. *Cell Death Differ.* **24**, 1214–1223 (2017).
10. Schmidt-Supprian, M. et al. Differential dependence of $CD4^+CD25^+$ regulatory and natural killer-like T cells on signals leading to NF-κB activation. *Proc. Natl Acad. Sci. USA* **101**, 4566–4571 (2004).
11. Smigiel, K. S. et al. CCR7 provides localized access to IL-2 and defines homeostatically distinct regulatory T cell subsets. *J. Exp. Med.* **211**, 121–136 (2014).
12. Long, M., Park, S.-G., Strickland, I., Hayden, M. S. & Ghosh, S. Nuclear factor-κB modulates regulatory T cell development by directly regulating expression of Foxp3 transcription factor. *Immunity* **31**, 921–931 (2009).
13. Oh, H. et al. An NF-κB transcription-factor-dependent lineage-specific transcriptional program promotes regulatory T cell identity and function. *Immunity* **47**, 450–465.e5 (2017).
14. Vasanthakumar, A. et al. The TNF receptor superfamily-NF-κB axis is critical to maintain effector regulatory T cells in lymphoid and non-lymphoid tissues. *Cell Rep.* **20**, 2906–2920 (2017).
15. Messina, N. et al. The NF-κB transcription factor RelA is required for the tolerogenic function of $Foxp3^+$ regulatory T cells. *J. Autoimmun.* **70**, 52–62 (2016).
16. Grinberg-Bleyer, Y. et al. NF-κB c-Rel is crucial for the regulatory T cell immune checkpoint in cancer. *Cell* **170**, 1096–1108.e13 (2017).
17. Yu, J. et al. Regulation of T-cell activation and migration by the kinase TBK1 during neuroinflammation. *Nat. Commun.* **6**, 6074 (2015).
18. Jenkins, M. H. et al. Multiple murine $BRaf^{V600E}$ melanoma cell lines with sensitivity to PLX4032. *Pigment Cell Melanoma Res.* **27**, 495–501 (2014).
19. Pierson, W. et al. Antiapoptotic Mcl-1 is critical for the survival and niche-filling capacity of $Foxp3^+$ regulatory T cells. *Nat. Immunol.* **14**, 959–965 (2013).
20. Overacre-Delgoffe, A. E. et al. Interferon-γ drives T_{reg} fragility to promote anti-tumor immunity. *Cell* **169**, 1130–1141.e11 (2017).
21. Gewies, A. et al. Uncoupling Malt1 threshold function from paracaspase activity results in destructive autoimmune inflammation. *Cell Reports* **9**, 1292–1305 (2014).
22. Jaworski, M. et al. Malt1 protease inactivation efficiently dampens immune responses but causes spontaneous autoimmunity. *EMBO J.* **33**, 2765–2781 (2014).
23. Bornancin, F. et al. Deficiency of MALT1 paracaspase activity results in unbalanced regulatory and effector T and B cell responses leading to multiorgan inflammation. *J. Immunol.* **194**, 3723–3734 (2015).
24. Nagel, D. et al. Pharmacologic inhibition of MALT1 protease by phenothiazines as a therapeutic approach for the treatment of aggressive ABC-DLBCL. *Cancer Cell* **22**, 825–837 (2012).
25. Schlauderer, F. et al. Structural analysis of phenothiazine derivatives as allosteric inhibitors of the MALT1 paracaspase. *Angew. Chem. Int. Edn Engl.* **52**, 10384–10387 (2013).
26. Fontan, L. et al. MALT1 small molecule inhibitors specifically suppress ABC-DLBCL *in vitro* and *in vivo*. *Cancer Cell* **22**, 812–824 (2012).
27. Wang, Y. et al. MALT1 promotes melanoma progression through JNK/c-Jun signaling. *Oncogenesis* **6**, e365 (2017).
28. Thome, M., Charton, J. E., Pelzer, C. & Hailfinger, S. Antigen receptor signaling to NF-κB via CARMA1, BCL10, and MALT1. *Cold Spring Harb. Perspect. Biol.* **2**, a003004–a003004 (2010).
29. Le, D. T. et al. PD-1 blockade in tumors with mismatch-repair deficiency. *N. Engl. J. Med.* **372**, 2509–2520 (2015).
30. Rizvi, N. A. et al. Cancer immunology. Mutational landscape determines sensitivity to PD-1 blockade in non-small cell lung cancer. *Science* **348**, 124–128 (2015).
31. Zaretsky, J. M. et al. Mutations associated with acquired resistance to PD-1 blockade in melanoma. *N. Engl. J. Med.* **375**, 819–829 (2016).

Acknowledgements We thank the MGH Pathology Flow Cytometry Core and N. Ali-Akbar for technical assistance. This study was funded by an EMBO fellowship (ALTF534-2015) and a Marie Curie Global Fellowship (750973) (M.D.P.), DFG Fellowships (PR 1652/1-1 to J.N.P and US 116/2-1 to S.M.U), NIH T32 CA207021 (V.M.), a Sara Elizabeth O'Brien Fellowship (F.M.), and Melanoma Research Alliance Senior Investigator Award MRA-348693, NIH AI123349, and the Bob and Laura Reynolds MGH Research Scholar Award (T.R.M.).

Reviewer information *Nature* thanks Shimon Sakaguchi and the other anonymous reviewer(s) for their contribution to the peer review of this work.

Author contributions M.D.P. initiated, designed, performed and analysed the experiments, and wrote the manuscript. E.Y.K. initiated the project, designed and performed experiments, V.Z. performed histological analyses, S.M.U. performed autoantibody assays, V.M. and F.M. performed T_{reg} cell analyses in lung and skin. F.M. performed in vitro T_{reg} suppression assay. E.C. generated tumour cell lines. M.N.N. and A.-C.V. performed RNA sequencing analyses, B.D.M. provided genetic mouse models, D.S. designed and performed RT–qPCR assay, B.L.C., S.M., J.N.P., R.D.W. and M.L. performed tumour growth studies and survival studies, T.R.M. conceived the study, supervised the project, designed experiments, and wrote the manuscript.

Competing interests M.D.P. and T.R.M. have filed a patent application (PCT/US2018/067856) related to the use of MALT1 inhibitors. T.R.M. is a co-founder of Monopteros Therapeutics. All other authors declare no competing interests.

Additional information
Extended data is available for this paper at https://doi.org/10.1038/s41586-019-1215-2.
Supplementary information is available for this paper at https://doi.org/10.1038/s41586-019-1215-2.
Reprints and permissions information is available at http://www.nature.com/reprints.
Correspondence and requests for materials should be addressed to M.D.P. or T.R.M.
Publisher's note: Springer Nature remains neutral with regard to jurisdictional claims in published maps and institutional affiliations.

METHODS

Mice. *Foxp3*$^{YFP\text{-}cre}$ (ref. [32]), *Foxp3*$^{GFP\text{-}creERT2}$ (ref. [33]), *ROSA26-stop*$^{f/f\text{-}YFP}$ (ref. [34]), *ROSA26-stop*$^{f/f\text{-}IKK2ca}$ (ref. [35]), *Ifng*$^{-/-}$[36], B6-*scurfy* (ref. [37]) and C57BL/6/J mice were purchased from Jackson Laboratories. R. J. Xavier and J. J. Moon provided *CARMA1*$^{f/f}$ (ref. [38]) and *Rag1*$^{-/-}$ mice, respectively. Animals were housed in specific-pathogen-free facilities at the Massachusetts General Hospital (MGH) and all experimental studies were approved and performed in accordance with guidelines and regulations implemented by the MGH Institutional Animal Care and Use Committee (IACUC). For survival studies, the age of mice at euthanasia mandated by a moribund state of health was recorded in Kaplan–Meyer plots.

Tumour cell lines. The *Braf*^{V600E} × *Pten*$^{-/-}$ melanoma cell line D4M.3A (ref. [18]) was provided by D. E. Fisher. For some experiments, D4M.3A cells were lentivirally transduced to express a blue fluorescent histone H2B-Cerulean fusion protein (D4M.3A-H2B-Cerulean), as previously described[39], to facilitate detection by flow cytometry. To generate D4M.3A-SIINFEKL tumours expressing the chicken ovalbumin-derived H-2K^{b}-restricted SIINFEKL peptide, we transduced D4M.3A cells with a VSV-G pseudotyped pHAGE-EF1α lentiviral vector engineered to express a fusion of histone H2B and Cerulean separated by two copies of the SIINFEKL minigene and its native flanking sequences in the ovalbumin protein to facilitate processing for antigen presentation. The colon adenocarcinoma cell line MC38[40] was obtained from A. D. Luster. All tumour lines were grown in DMEM with 10% fetal calf serum (FCS) and used for experiments when in exponential growth phase.

Tumour growth studies and treatments. One million D4M.3A, D4M.3A-H2B-Cerulean, D4M.3A-SIINFEKL or MC38 tumour cells were injected subcutaneously in 100 μl HBSS without Ca^{2+} into the flanks of mice. Wherever possible, animals were randomized into treatment groups. Tumour volumes were measured every second to third day after the start of treatments and calculated as $V = (\text{length} \times \text{width}^2)/2$.

Tamoxifen (1 mg per mouse in 100 μl of a 9:1 mixture of olive oil and ethanol) was injected intraperitoneally daily as indicated. FTY720 (1 mg kg^{-1} bodyweight) in 150 μl H_2O was injected intraperitoneally every other day until the end of the experiment. Anti-IFNγ antibody (500 μg per mouse; clone XMG1.2) was injected intraperitoneally on day 14 after birth or on the day of tumour implantation and then every other day thereafter until the end of the experiment. Anti-PD-1 (200 μg; clone 29F.1A12) or rat IgG2a isotype control (200 μg; clone 2A3) was injected intraperitoneally three times in 100 μl PBS every other day at the indicated time points. Anti-CD8α (150 μg; clone YTS169.4) was injected in 100 μl PBS every other day from the indicated time point until the end of the experiment. Mepazine (16 mg kg^{-1} bodyweight in 5% dimethylsulfoxide (DMSO)) or MI-2 (20 mg kg^{-1} in 5% DMSO in purfied H_2O) was injected intraperitoneally daily starting at the indicated time points until the end of the experiment, unless indicated otherwise. For adoptive T_{reg} cell transfer studies, CD4$^+$ YFP$^+$ T_{reg} cells were purified to more than 95% purity through magnetic-activated cell sorting (Miltenyi) from LNs and spleen of *F*^{cre} × *C1*$^{f/+}$ or *C1*$^{+/+}$ mice and 10^6 cells per mouse were injected intravenously into the tail vein the day before tumour implantation.

Preparation of single-cell suspensions, antibody staining and flow cytometry. Heparinized peripheral blood collected through sub-mandibular vein puncture was treated with ACK red blood cell lysis buffer. LNs and spleens were passed through 40-μm cell strainers, followed by red blood cell lysis (spleens only). Tumours and lung tissue were minced into small fragments and treated with 1.5 mg ml^{-1} collagenase IV and 50 U ml^{-1} DNase I for 30 min at 37 °C under agitation. Skin tissue was digested in medium containing 2% FCS, 10 mM HEPES, 0.5 mg ml^{-1} hyaluronidase, 1.5 mg ml^{-1} collagenase IV, and 50 U ml^{-1} DNase I for 45 min at 37 °C under agitation. Residual tissue fragments were mechanically dissociated.

Cell surface proteins were stained for 20 min at 4 °C with the following antibodies against: CD11b (M1/70), CD120b/TNFR2 (polyclonal Armenian hamster IgG), CD274/PD-L1 (10F.9G2), CD357/GITR (DTA-1), CD4 (GK1.5), CD45 (30-F11), CD62L (MEL-14), CD73 (TY/11.8), CD8α (53-6.7), CD90.2 (30-H12), F4/80 (BM8), H-2K^{b} (AF6-88.5), -I-A/I-E (M5/114.15.2), Ly-6C (HK1.4), Ly-6G (1A8), CD45R/B220 (RA3-6B2), CD64 (FcγRI) (X54-5/7.1), CD11c (N418), CD103 (2E7), NK-1.1 (PK136), CD335 (NKp46) (29A1.4), CD3 (17A2), CD19 (1D3/CD19), CD45RB (16A), and CD44 (IM7) (BioLegend), CD11c (HL3) and CD25 (PC61.5) (eBIoscience).

Intracellular and nuclear proteins were stained for 60 min at room temperature after permeabilization and fixation (Mouse regulatory T cell staining Kit; eBioscience) using antibodies against: CD152/CTLA-4-(UC10-4B9), TNF (MP6-XT22), IL-4 (11B11), IL-17A (TC11-18H10.1), IFNγ (XMG1.2), T-bet (4B10), and Ki67 (16A8) (BioLegend), BIM (C34C5), CARD11/CARMA1 (1D12) (Cell Signaling), FOXP3 (FJK-16 s, eBioscience), GATA-3 (L50-823) and Ki67 (B56) (BD Biosciences), RORγt (AFKJS-9) and GFP (rabbit polyclonal) (Invitrogen). Polyclonal goat anti-rabbit Ig (H+L) secondary antibody (Life Technologies) was used to reveal primary anti-CARMA1 staining.

Preceding antibody staining, dead cells were stained using the fixable viability violet dye Zombie Red (Biolegend) for 15 min at room temperature, followed by blocking of Fc receptors with TruStain FcX (Biolegend) for 20 min at 4 °C. Cells were analysed on LSR II, LSRFortessa or LSRFortessa X-20 flow cytometers (BD Biosciences), and data were analysed with FlowJo software v.9.9.5.

Phospho-protein analysis. LN single-cell suspensions were stained using the fixable viability dye ZombieRed (Biolegend) for 15 min at room temperature, and added for 30 min at 37 °C to tissue culture plates pre-coated overnight with anti-CD3ε (clone 145-2C11) and anti-CD28 (clone 37.51) antibodies (at 10 μg ml^{-1} of each antibody), or to uncoated control plates. Samples were then fixed in 4% paraformaldehyde (PFA) for 10 min at room temperature, and permeabilized for 20 min through dropwise addition of 1 ml ice-cold methanol. Cells were then stained for CD90.2 (30-H12), CD4 (GK1.5), CD8α (53-6.7), CD44 (IM7) (BioLegend), Foxp3 (FJK-16 s, eBioscience), pFoxo1 (Thr24)/Foxo3a (Thr32), p-c-Jun (Ser73) (D47G9) (Cell Signaling) and GFP (rabbit polyclonal Ab) (Invitrogen).

Analysis of in situ and ex vivo stimulated cytokine secretion. To detect in situ cytokine secretion, mice were slowly injected intravenously with 500 μg of brefeldin A in 250 μl PBS 6 h before euthanization and intracellular cytokine staining.

To detect cytokine secretion in T cells upon ex vivo re-stimulation, single-cell suspensions from tumours and LNs were resuspended in RPMI 1640 with 10% FCS and added to anti-CD3 (clone 145-2C11)/anti-CD28 (clone 37.51) antibody-coated (overnight at 10 μg ml^{-1} antibody) tissue culture plates for 8 h at 37 °C in the presence of 1 μg ml^{-1} Golgiplug and Monensin (both from Biolegend) and cells processed for intracellular cytokine staining.

Analysis of exT_{reg} cells. CD4$^+$ YFP^{bright} cells were first purified by FACS from LNs and spleens of *Foxp3*$^{YFP\text{-}cre/+}$ × *CARMA1*$^{f/f}$ (or $^{f/+ \text{ or } +/+}$) × *ROSA26*^{YFP} mice and stained for FOXP3 expression for flow cytometry analysis, as described above.

In vivo and in vitro suppression. For in vivo suppression studies, 3 × 10^5 Miltenyi (negative selection) enriched CD4$^+$ and FACS sorted (>98% purity) CD45RB^{high} YFP$^-$ cells from LNs and spleens of *Foxp3*$^{YFP\text{-}cre/cre}$ mice were intravenously injected into the tail vein of *Rag1*$^{-/-}$ mice with or without 1 × 10^5 Miltenyi (negative selection) enriched CD4$^+$ and FACS sorted (>98% purity) YFP^{bright} T_{reg} cells from LNs and spleens of *Foxp3*$^{YFP\text{-}cre/+}$ × *CARMA1*$^{f/f}$ (or *CARMA1*$^{f/+}$ or *CARMA1*$^{+/+}$) × *ROSA26*^{YFP} mice.

For in vitro suppression studies, 1 × 10^4 FACS-sorted (>98% purity) CD4$^+$ YFP$^-$ conventional T cells from LNs and spleens of *Foxp3*$^{YFP\text{-}cre/cre}$ mice were labelled with 5 μM CellTrace Violet and stimulated with 250 ng ml^{-1} of anti-CD3 monoclonal antibody (145-2c11, Biolegend) in presence of 2.5 × 10^4 T-cell depleted splenocytes and different concentrations (from 1:1 to 1:16) of Miltenyi (negative selection) enriched CD4$^+$ and FACS sorted (>98% purity) YFP^{bright} Treg cells from LNs and spleens of *Foxp3*$^{YFP\text{-}cre/+}$ × *CARMA1*$^{f/f}$ (or *CARMA1*$^{f/+}$ or *CARMA1*$^{+/+}$) × *ROSA26-stop*$^{f/f\text{-}YFP}$ mice. CD4$^+$ YFP$^-$ conventional T cell proliferation was read out after 72 h, as previously described[41]. In brief, percentage of suppression was scaled from 0 (proliferation of conventional T cell in absence of T_{reg} cells) to 100 (complete absence of proliferation).

In vitro apoptosis. Enriched CD4$^+$ and FACS-purified (>99% purity) YFP^{bright} T_{reg} cells from LNs of *Foxp3*$^{YFP\text{-}cre/+}$ × *CARMA1*$^{f/f}$ (or *CARMA1*$^{+/+}$) × *ROSA26-stop*$^{f/f\text{-}YFP}$ mice were added for 6 and 18 h at 37 °C to tissue culture plates pre-coated overnight with anti-CD3ε (clone 145-2C11) and anti-CD28 (clone 37.51) antibodies (at 10 μg ml^{-1} of each antibody). Viability of CD44^{low}CD62L$^+$ cT_{reg} and CD44^{high}CD62L$^-$ eT_{reg} cells was then read out by annexin V and Zombie Red staining (Biolegend).

RNA sequencing studies: sample collection. CD4$^+$ T cells from LNs and spleens of *F*$^{cre/+}$ × *C1*$^{+/+}$, *C1*$^{f/+}$ or *C1*$^{f/f}$ mice were pre-enriched by immunomagnetic cell sorting (Miltenyi negative selection) and then 5 × 10^3 YFP$^+$CD4$^+$CD44^{low}CD62L$^+$ cT_{reg} cells per animal and the same number of YFP$^+$CD4$^+$CD44^{high}CD62L$^-$ eT_{reg} cells were sorted to >99% purity directly into 10 μl lysis buffer consisting of TCL buffer (Qiagen) and 1% of β-mercaptoethanol. Samples were then flash-frozen and kept at −80 °C before further processing following a modified version of the Smart-Seq2 protocol[11,12,14], as described below. A total of 18 samples was collected, but 2 samples were discarded for technical reasons.

Reverse transcription. Samples were thawed on ice for 2 min, and then centrifuged at 2,500 rpm at 4 °C for 1 min and the RNA concentration normalized. RNA (1.9 μl per sample) was moved to a full-skirt 96-well plate (Eppendorf). Each sample was then mixed with 1 μl 10 μM RT primer 5′-AAGCAGTGGTATCAACGCAGAGTACTTTTTTTTTTTTTTTTTTTTTTTTTTTTTTVN-3′ (IDT), 1 μl 10 mM dNTP (Life Technologies/Thermo Fisher Scientific), and 0.1 μl SUPERase·In RNase-Inhibitor (20 U μl^{-1}, Life Technologies/Thermo Fisher Scientific). Samples were denatured at 72 °C for 3 min using an Eppendorf Mastercycler and placed immediately on ice afterwards. The Reverse Transcription Mix (7 μl) was subsequently added to every well, consisting of: 2 μl 5× RT buffer (Thermo Fisher Scientific), 2 μl 5 M betaine (Sigma-Aldrich), 0.9 μl 100 mM $MgCl_2$ (Sigma-Aldrich), 1 μl 10 μM TSO (5′-AAGCAGTGGTATCAACGCAGAGTACATrGrG+G-3′, Exiqon), 0.25 μl

SUPERase·In RNase-Inhibitor (20 U μl^{-1}, Life Technologies/Thermo Fisher Scientific), 0.1 μl Maxima H Minus Reverse Transcriptase (200 U μl^{-1}, Thermo Fisher Scientific) and 0.75 μl nuclease-free water. Reverse transcription was carried out by incubating the plate at 50 °C for 90 min, followed by heat inactivation at 85 °C for 5 min.

PCR pre-amplification and cDNA purification. PCR Mix (14 μl, consisting of 0.5 μl 10 μM PCR primer 5′-AAGCAGTGGTATCAACGCAGAGT-3′ (IDT), 12.5 μl 2× KAPA HiFi HotStart ReadyMix (KAPA Biosystems) and 1 μl nuclease-free water) was added to each well for a final PCR reaction volume of 25 μl. The reaction was carried out with an initial incubation at 98 °C for 3 min, followed by 16 cycles at 98 °C for 15 s, 67 °C for 20 s, and 72 °C for 6 min, and a final extension at 72 °C for 5 min. PCR products were purified by mixing them with 20 μl (0.8×) of Agencourt AMPureXP SPRI beads (Beckman-Coulter), followed by a 6-min incubation period at room temperature. The plate was then placed onto a magnet for 6 min before removing the supernatant. SPRI beads were washed twice with 100 μl of freshly prepared 70% ethanol, with care being taken to avoid loss of beads during the washes. After removing all residual ethanol traces, SPRI beads were left to dry at room temperature for 10 min. The beads were then resuspended in 20 μl of TE buffer (Teknova) and incubated at room temperature for 5 min. The plate was placed on the magnet for 5 min before transferring the supernatant containing the amplified cDNA to a new 96-well plate. This cDNA SPRI clean-up procedure was repeated a second time to remove all residual primer dimers. The concentration of amplified cDNA was measured on the Synergy H1 Hybrid Microplate Reader (BioTek) using the Qubit dsDNA High Sensitivity Assay Kit (Life Technologies/Thermo Fisher Scientific). The cDNA size distribution of few selected wells was assessed on a High-Sensitivity Bioanalyzer Chip (Agilent), and the expected size distribution sharply peaked around 2 kb.

Sequencing library preparation. Library preparation was carried out using the Nextera XT DNA Sample Kit (Illumina) with custom indexing adapters, allowing the 18 libraries to be simultaneously generated in a 384-well PCR plate (Eppendorf). For each library, the amplified cDNA was normalized to a 0.15–0.20 ng μl^{-1} concentration range. The tagmentation reaction consisted of mixing 0.625 μl of normalized cDNA with 1.25 μl of Tagmentation DNA (TD) buffer and 0.625 μl of Amplicon Tagment enzyme Mix (ATM). The 2.5-μl reaction was incubated at 55 °C for 10 min and then immediately placed on ice upon completing this incubation step. The reaction was quenched with 0.625 μl of Neutralize Tagment (NT) buffer and incubated at room temperature for 10 min. The libraries were amplified by adding 1.875 μl of Nexstera PCR Master (NPM) Mix, 0.625 μl of 10 μM i5 adaptor 5′-AATGATACGGCGACCACCGAGATCTACAC[i5]TCGTCGGCAGCGTC-3′ (IDT), in which [i5] signifies the 8-bp i5 barcode sequence (see below for sequences), and 0.625 μl of 10 μM i7 adaptor 5′CAAGCAGAAGACGGCATACGAGAT[i7] GTGACTGGAGTTCAGACGTGTGCTCTTCCGATCTGGG-3′ (IDT), in which [i7] represents the reverse-complement of the 8-bp i7 barcode sequence (see below for sequences used). The PCR was carried out at an initial incubation at 72 °C for 3 min, 95 °C for 30 s, followed by 12 cycles of (95 °C for 10 s, 55 °C for 30 s, 72 °C for 1 min), and a final extension at 72 °C for 5 min. Following PCR amplification, 2.5 μl of each library were pooled together in a 1.5-ml Eppendorf tube. The pool was mixed with 67.5 μl (0.9× ratio for 2.5 μl of 30 samples pooled together) of Agencourt AMPureXP SPRI beads (Beckman-Coulter) and incubated at room temperature for 5 min. The pool was then placed on a magnet (DynaMag-2, Life Technologies) and incubated for 5 min. The supernatant was removed and the SPRI beads were washed twice with 1 ml of freshly prepared 70% ethanol. After removing all residual ethanol traces, the SPRI beads were left to dry at room temperature for 10 min. The beads were resuspended in 100 μl of nuclease-free water and incubated at room temperature for 5 min. The tube was then placed back on the magnet for 3 min before transferring the supernatant to a new 1.5-ml Eppendorf tube. This SPRI clean-up procedure of the library was repeated a second time to remove all residual primer dimers, using the same approach. The concentration of the pooled libraries was measured using the Qubit dsDNA High Sensitivity Assay Kit (Life Technologies/Thermo Fisher Scientific), and the library size distribution measured on a High-Sensitivity Bioanalyzer Chip (Agilent), showing the expected size distribution of 300–500 bp. The 18 pooled samples were sequenced as paired-end on an Illumina NextSeq 500 instrument using the NextSeq 500/550 High Output v2 kit (75 cycles).

i5 barcodes: AAGTAGAG, ACACGATC, TGTTCCGA. i7 barcodes: GAATTGCT, GTCAAGTT, ATCCGACA, CAAGGCGA, AGTGTCTT, GACCGAGA.

RNA sequencing analysis. Raw sequencing reads were demultiplexed and converted to FASTQ files using Illumina bcl2fastq2 Illumina software (version 2.17.1.14). FASTQ sequencing reads were then aligned to mm10 reference genome using the STAR aligner with default parameters[42]. RSEM (v.1.2.8) was used to quantify gene expression level from aligned reads and generate count expression matrices for each experimental condition[43]. We filtered out lowly expressed genes with a count per million (CPM) < 0.5 in more than two conditions, leaving a total of 14,168 genes for further analysis. The distribution of $\log_2$ normalized CPM data was visualized to assess for coverage, and all conditions had similar distributions.

Gene expression analysis. Gene expression matrices were analysed using the limma package in R[44]. The global topology of quantile normalized data was visualized using the multidimensional scaling (plotMDS) function in limma after removing batch effects using the removebatchEffect function in limma with default parameters taking into account design and batch matrices. Differential gene expression was performed using empirical Bayesian statistics (eBayes) function in limma simultaneously correcting for batch using blocking terms for batch covariates. Differentially expressed genes with log fold change greater than 1 and a P value below cut-off were visualized using the heatmap.2 function in gplots. All P values were corrected for multiple hypothesis testing using Benjamini–Hochberg correction. For R scripts used to perform the gene expression analyses see Supplementary Methods. The same differential expression steps were used to re-analyse the gene expression data from GEO accession GSE82008 to obtain the list of differentially expressed genes between c-Rel and p65 knockout versus wild-type resting and activated T_{reg} cells. A list of 831 'eTreg signature' genes from ref. [16] was obtained by direct correspondence with the authors. Overlap between differentially expressed genes, including the list of eT_{reg} cell signatures from the current study and ref. [16], was visualized using the vennDiagram function in limma.

Quantitative RT–PCR. For analysis of gene expression, RNA was isolated (AllPrep, DNA/RNA Mini kit; Qiagen) from $CD4^+$ GFP^+ T_{reg} cells sorted to >99% purity from tdLNs and tumours, or from homogenized tumour tissue, and reverse transcribed using iScript cDNA Synthesis Kit (Bio-RAD). Quantitative reverse transcription (RT–PCR) was performed using iQ SYBR green supermix (Bio-RAD) and primers: *CARMA1* Fwd 5′-ACATGCTGAGCCGTTACATCA-3′, *CARMA1* Rev 5′-CCACATAGCCCCTTTGTCCC-3′, *Ifng* Fwd 5′-CGGCACAGT CATTGAAAGCCTA-3′, *Ifng* Rev 5′-GTTG CTGATGGCC TGATTGTC-3′, *Ctla4* Fwd 5′-GCTTCCTAGATTACCCCTTCTGC-3′, *Ctla4* Rev 5′-CGGGCATGG TTCTGGATCA-3′, *CD25*-Fwd 5′-CCACATTCAAAGCC CTCTCCTA-3′, CD25-Rev 5′-GTTTTCCCACACTTCATCTTGC-3′, *Foxp3* Fwd 5′-TTGG CCAGCGCCA TCTT-3′, *Foxp3* Rev 5′-TGCCTCCTCCAGAGAGAAGTG-3′, *GITR* (also known as *Tnfrsf18*) Fwd 5′-AAGGTTCAGAACGGAAGTG-3′, *GITR* Rev 5′-GGGTCTCCACAGTGGTACT-3′, *CD73* (also known as *Nt5e*) Fwd 5′-CAA ATCCCACACAACCACTG-3′, *CD73* Rev 5′-TGCTCACTTGGTCACA GGAC-3′, *Gzmb* Fwd 5′-CATGTAGGGTCGAGAGTGGG-3′, *Gzmb* Rev 5′-CCTCCTGC TACTGCTGAC CT-3′, *Pdl1* (also known as *Cd274*) Fwd 5′-TGCTGCATAATCAGCTACGG-3′, *Pdl1* Rev 5′-GCTGGTCACATT GAGAAGCA-3′, *Socs1*-Fwd 5′-ACAAGCTGCTACAACCAGG G-3′, *Socs1* Rev 5′-ACT TCTGGCTGGAGACCTCA-3′, *Tap1* Fwd 5′-GTGGCCGCAGTG GGA CAAGAG-3′, *Tap1* Rev 5′-AGGGCACTGGTGGCATCATC-3′, *Stat1* Fwd 5′-TGGTGAAATTGCAAG AGCTG-3′, *Stat1* Rev 5′-CAGACTTCCG TTGGTGGATT-3′, *Irf1* Fwd 5′-CAG AGGAAAG AGAGAAAGTCC-3′, *Irf1* Rev 5′-CACACGGTGACAGTGCTGG, *Cxcl10* Fwd 5′-CATC CTGCTGGGT CTGAGTG-3′, *Cxcl10*-Rev 5′-ATTCTCACTGGCCCGTCATC, *Nos2* Fwd 5′-CAAGAGAGTGCTGTTCCAGGT-3′ and *Nos2* Rev 5′-GAGCACGCTGAGT ACC TCATT-3′, *Gapdh* Fwd 5′-TGGTGAAGGTCGGTGAAC-3′ and *Gapdh* Rev 5′-CC ATGTAGTTGAGGTCAATGAAGG-3′. Results were expressed as $2^{-\Delta Ct}$ relative to the house keeping gene *Gapdh*.

Histology. Tissue samples obtained from all organs were fixed in 10% buffered formalin for 48 h, trimmed and placed into microcassettes, and embedded in paraffin wax. Sections of 5 μm were stained with haematoxylin and eosin according to standard procedures.

Immunofluorescence. Kidney, liver, and stomach from a *Rag1*$^{-/-}$ mouse were embedded in OCT and flash-frozen in cold methylbutane equilibrated on dry ice. Sections of 10 μm were permeabilized with pre-cooled 90% methanol for 10 min at −20 °C, blocked in TruStain FcX (93, Biolegend) with 1% goat serum and 0.25% BSA in PBS for 60 min, incubated with sera (1:100 dilution) from *Foxp3*$^{YFP\text{-}cre}$ × *CARMA1*$^{f/f}$ (or *CARMA1*$^{f/+}$ or *CARMA1*$^{+/+}$) mice for 120 min and stained with anti-mouse IgG (H+L)-Alexa Fluor 647 (1:500) (A-21235, Thermo Fisher) and DAPI (Sigma) for 120 min. Sections were mounted on coverslips in Prolong (Thermo Fisher) and imaged with LSM 780 AxioObserver confocal microscope (Carl Zeiss) using a 20× lens (Apochromat, 0.8 W).

Statistical analysis. A two-tailed Student's t-test was used for comparisons between two groups, and a two-way ANOVA with Bonferroni post hoc test (multiple time points) or one-way ANOVA with Tukey post hoc test (single time points) was used for comparisons across multiple groups, unless otherwise indicated. A log-rank (Mantel–Cox) test was used to compare survival curves. All statistical tests were performed with GraphPad Prism software, and $P < 0.05$ was considered statistically significant. No statistical methods were used to predetermine sample size. Investigators were not blinded to allocation during experiments and outcome assessment.

Reporting summary. Further information on research design is available in the Nature Research Reporting Summary linked to this paper.

Data availability

All datasets generated during the current study are available from the corresponding authors upon reasonable request. RNA sequencing data have been deposited at the Gene Expression Omnibus (GEO) under accession number GSE129480.

32. Rubtsov, Y. P. et al. Regulatory T cell-derived interleukin-10 limits inflammation at environmental interfaces. *Immunity* **28**, 546–558 (2008).
33. Rubtsov, Y. P. et al. Stability of the regulatory T cell lineage in vivo. *Science* **329**, 1667–1671 (2010).
34. Srinivas, S. et al. Cre reporter strains produced by targeted insertion of *EYFP* and *ECFP* into the *ROSA26* locus. *BMC Dev. Biol*. **1**, 4 (2001).
35. Sasaki, Y. et al. Canonical NF-κB activity, dispensable for B cell development, replaces BAFF-receptor signals and promotes B cell proliferation upon activation. *Immunity* **24**, 729–739 (2006).
36. Dalton, D. K. et al. Multiple defects of immune cell function in mice with disrupted interferon-γ genes. *Science* **259**, 1739–1742 (1993).
37. Godfrey, V. L., Wilkinson, J. E., Rinchik, E. M. & Russell, L. B. Fatal lymphoreticular disease in the scurfy (sf) mouse requires T cells that mature in a sf thymic environment: potential model for thymic education. *Proc. Natl Acad. Sci. USA* **88**, 5528–5532 (1991).
38. Egawa, T. et al. Requirement for CARMA1 in antigen receptor-induced NF-κB activation and lymphocyte proliferation. *Curr. Biol*. **13**, 1252–1258 (2003).
39. Marangoni, F. et al. The transcription factor NFAT exhibits signal memory during serial T cell interactions with antigen-presenting cells. *Immunity* **38**, 237–249 (2013).
40. Spiess, P. J., Yang, J. C. & Rosenberg, S. A. In vivo antitumor activity of tumor-infiltrating lymphocytes expanded in recombinant interleukin-2. *J. Natl. Cancer Inst.* **79**, 1067–1075 (1987).
41. Marangoni, F. et al. Tumor tolerance-promoting function of regulatory T cells is optimized by CD28, but strictly dependent on calcineurin. *J. Immunol*. **200**, 3647–3661 (2018).
42. Dobin, A. et al. STAR: ultrafast universal RNA-seq aligner. *Bioinformatics* **29**, 15–21 (2013).
43. Li, B. & Dewey, C. N. RSEM: accurate transcript quantification from RNA-Seq data with or without a reference genome. *BMC Bioinformatics* **12**, 323 (2011).
44. Ritchie, M. E. et al. limma powers differential expression analyses for RNA-sequencing and microarray studies. *Nucleic Acids Res*. **43**, e47 (2015).

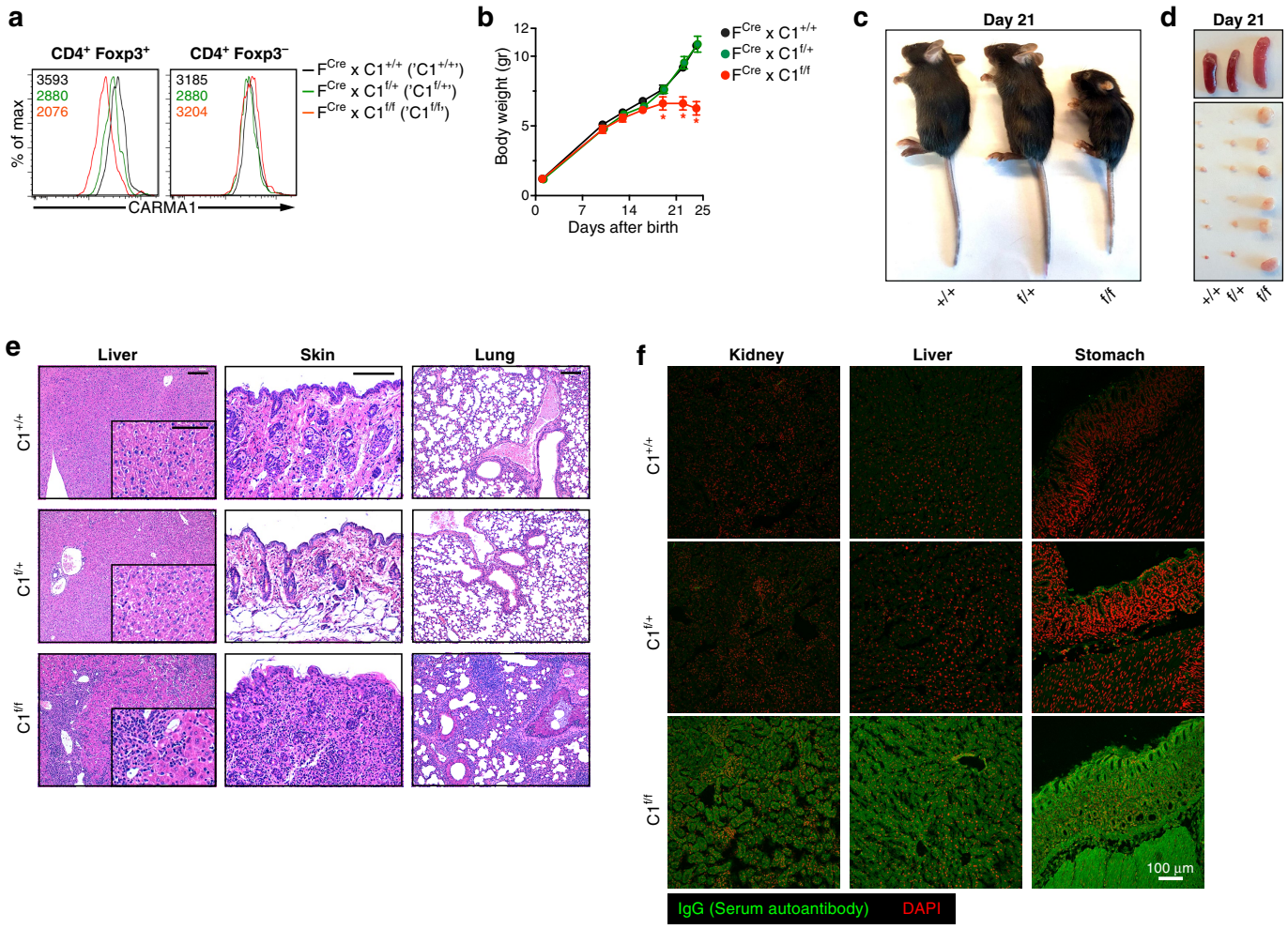

Extended Data Fig. 1 | Lymphoproliferative disease after T_{reg}-cell-specific deletion of CARMA1. a, CARMA1 protein in T_{reg} cells and $CD4^+$ T_{conv} cells from LNs of $F^{cre} \times C1^{+/+}$, $C1^{f/+}$ and $C1^{f/f}$ mice. **b**, Weight curves ($n = 5$ per group). **c**, **d**, Appearance of 21-day-old mice (**c**), and their spleens and LNs (**d**). **e**, Histological appearance of liver, skin and lung at 21 days of age of indicated mice. Scale bars, 150 μm and 50 μm (insets). **f**, Kidney, liver and stomach tissue sections of healthy C57BL/6 $Rag1^{-/-}$ mice were reacted with serum from 21-day-old mice of the indicated genotypes, and self-tissue-reactive IgG revealed by anti-mouse IgG staining (green). Nuclei were stained with DAPI (red). In **b**, $^*P < 0.05$ versus $C1^{+/+}$ and $C1^{f/+}$ (two-way ANOVA with Bonferroni post hoc test).

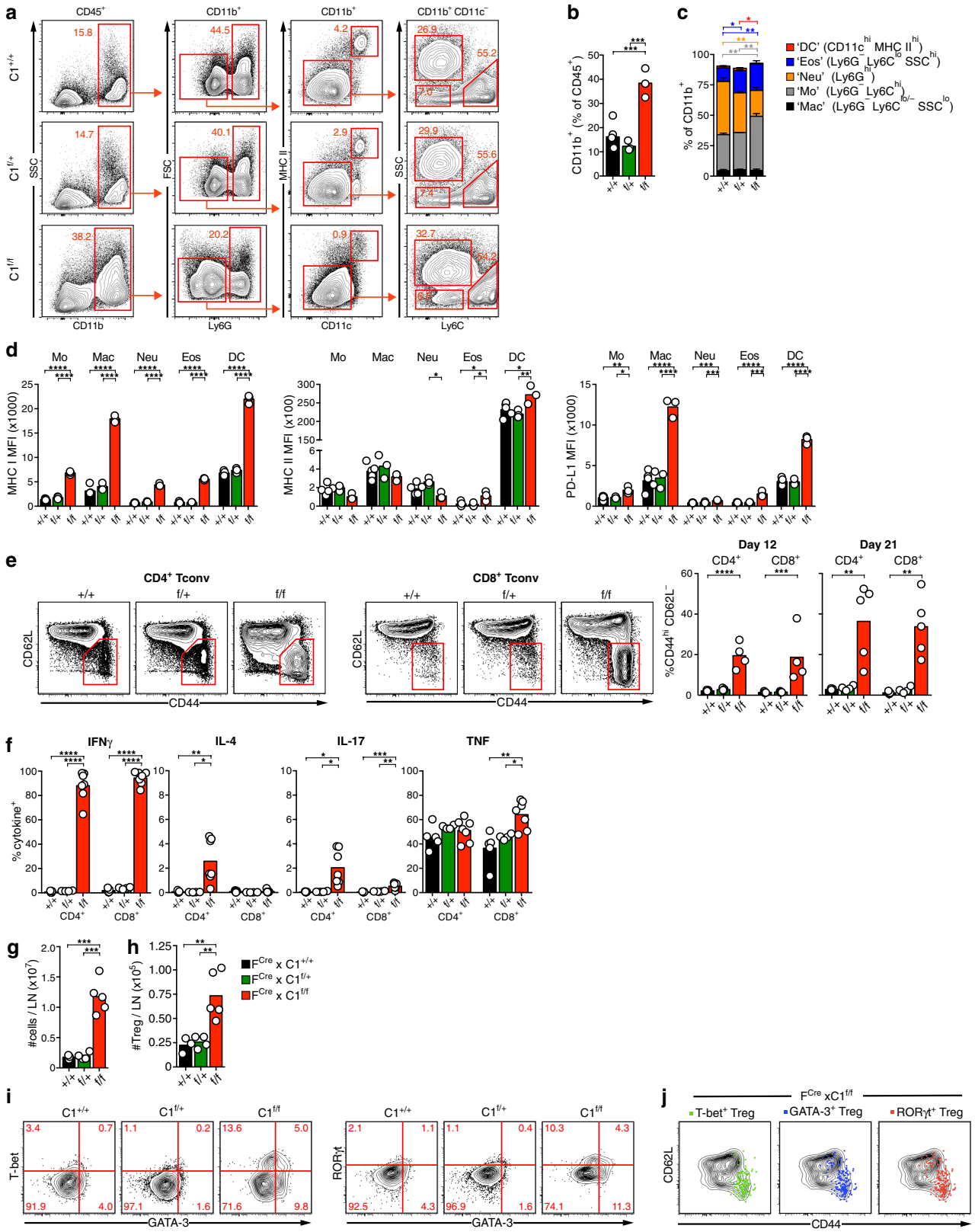

Extended Data Fig. 2 | Myeloid cell expansion and effector cytokine secretion by T_{conv} and T_{reg} cells after T_{reg}-cell-specific deletion of CARMA1. a–**c**, Size of the $CD11b^+$ splenic myeloid compartment and proportions of $Ly6G^+$ neutrophils, $CD11c^+MHC\ II^{high}$ dendritic cells (DCs), $Ly6C^{high}$ monocytes, $Lyc6G^{low}SSC^{high}$ eosinophils, and $Ly6C^{low}SSC^{low}$ macrophages in $F^{cre} \times C1^{+/+}$, $C1^{f/+}$ or $C1^{f/f}$ mice. **d**, Expression of MHC-I, MHC-II and PD-L1 on splenic myeloid subsets. **e**, Frequency of $CD4^+$ and $CD8^+$ T_{conv} cells with a $CD44^{high}CD62L^-$ effector memory phenotype in LNs of indicated mice at age 12 and 21 days. **f**, Effector cytokine expression of T_{conv} cells from 21-day-old mice after 8-h ex vivo stimulation on anti-CD3/CD28-coated plates. **g**, LN cellularity. **h**, Absolute numbers of T_{reg} cells in LNs. **i**, Co-expression of indicated transcription factors by T_{reg} cells from LNs of indicated mice. **j**, Expression of CD44 and CD62L by $F^{cre} \times C1^{f/f}$ T_{reg} cells expressing T-bet (green dots), GATA-3 (blue dots), or RORγt (red dots), compared to total $C1^{f/f}$ T_{reg} cells (contour plots). $^*P < 0.05$, $^{**}P < 0.01$, $^{***}P < 0.001$, $^{***}P < 0.0001$ (one-way ANOVA with Tukey post hoc test).

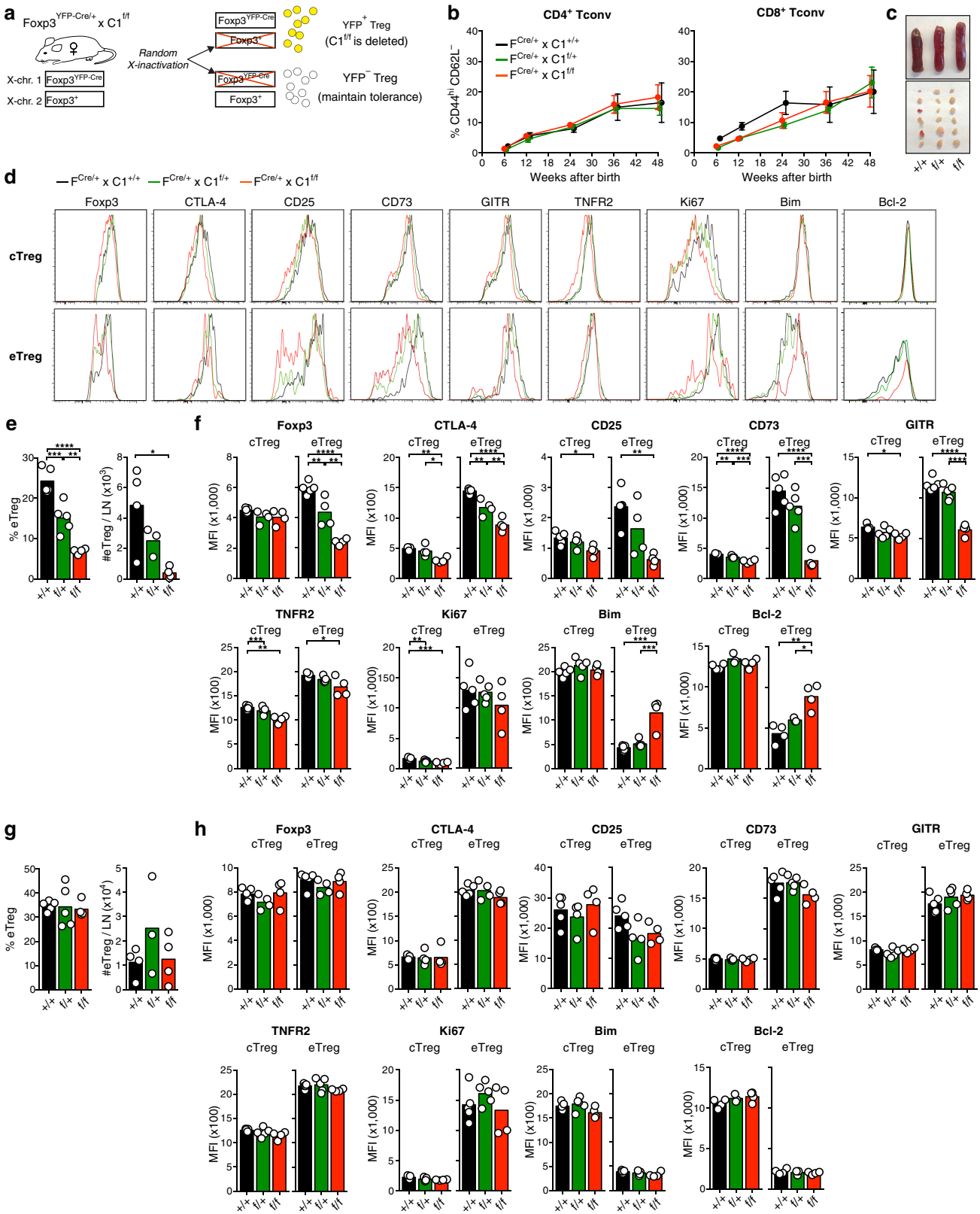

Extended Data Fig. 3 | Role of CARMA1 in eT_{reg} cell differentiation. **a**, Female heterozygous $F^{cre/+} \times C1^{f/f}$ mice express YFP–Cre and delete $C1^{f/f}$ in half of the T_{reg} cells owing to X-chomosomal location of the $Foxp3^{YFP\text{-}cre}$ allele and random X chromosome inactivation, whereas the other half of the T_{reg} cells remains functional. **b**, Frequency of $CD4^+$ and $CD8^+$ T_{conv} cells with a $CD44^{high}CD62L^-$ effector memory phenotype in peripheral blood of ageing $F^{cre/+} \times C1^{+/+}$, $C1^{f/+}$ or $C1^{f/f}$ mice ($n = 4$ per group). **c**, Appearance of spleens and LNs of indicated mice at one year of age. **d**–**f**, Frequency and absolute numbers (**e**) of eT_{reg} cells and expression of FOXP3, indicated markers of eT_{reg} cell differentiation, as well as proliferation marker Ki67, pro-apoptotic protein BIM and anti-apoptotic protein BCL2 by YFP^+ cT_{reg} and eT_{reg} cells (**d**, **f**) from nine-week-old $F^{cre/+} \times C1^{+/+}$, $C1^{f/+}$ or $C1^{f/f}$ mice. Note that some data on eT_{reg} cells in **e** and **f** are also shown in Fig. 1g, h and shown here to facilitate the comparison to cT_{reg} and YFP^- T_{reg} cells in **g** and **h**. **g**, **h**, Frequency and absolute numbers of eT_{reg} cells (**g**) and eT_{reg} cell markers on YFP^- cT_{reg} and eT_{reg} cells (**h**) from the same mice as shown in **d** and **f**. $^*P < 0.05$, $^{**}P < 0.01$, $^{***}P < 0.001$, $^{***}P < 0.0001$ (one-way ANOVA with Tukey post hoc test).

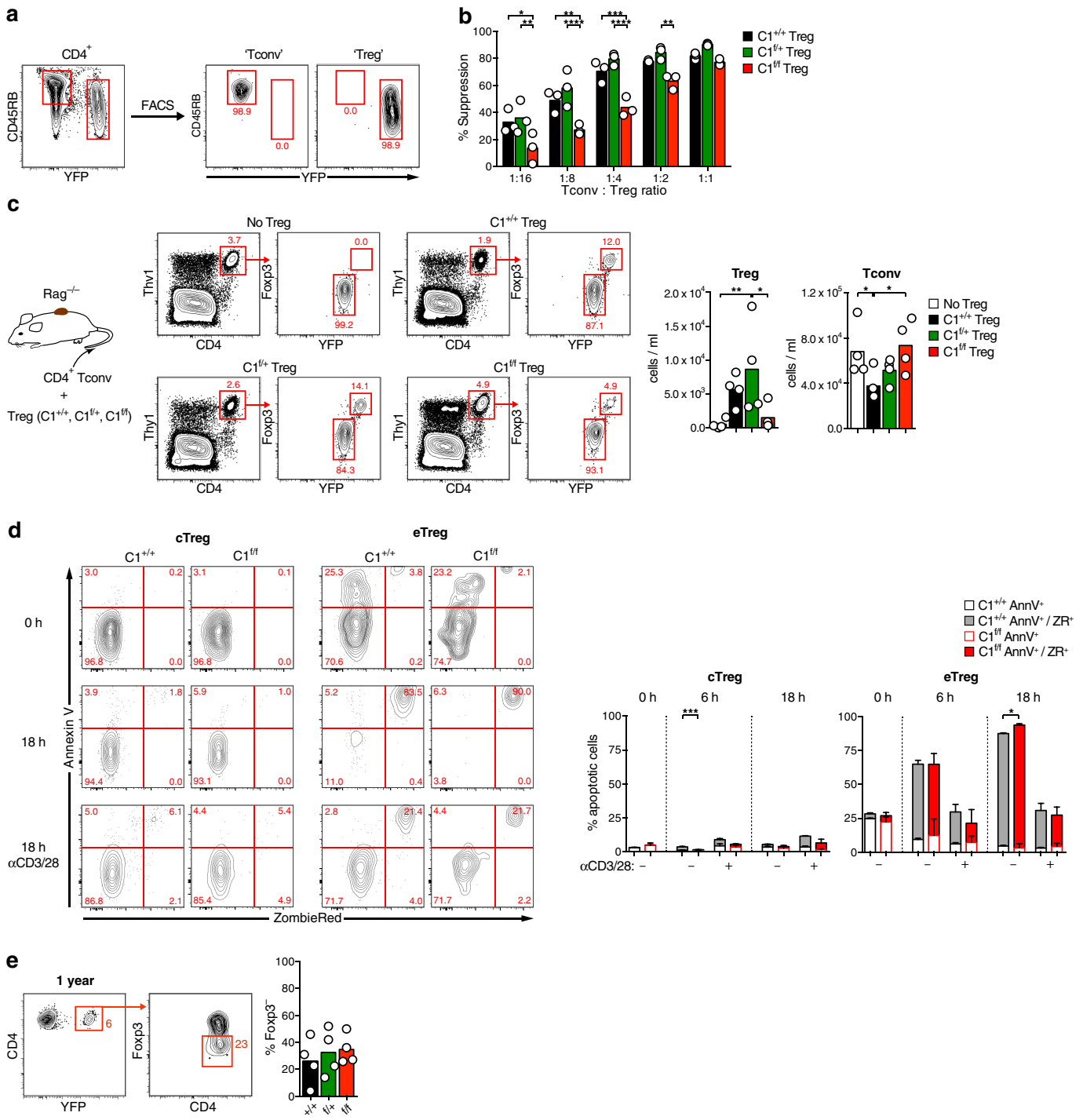

Extended Data Fig. 4 | In vitro and in vivo suppression, apoptotic rate and exT_{reg} cell formation of CARMA1-deficient T_{reg} cells. **a**, $CD4^+CD45RB^{high}YFP^-$ T_{conv} cells and $CD4^+CD45RB^{low}YFP^{bright}$ T_{reg} cells were double-sorted to more than 98% purity from LNs and spleens of $F^{cre} \times C1^{+/+} \times ROSA26\text{-}stop^{f/f\text{-}YFP}$ mice, which allow for clear differentiation of Cre-expressing T_{reg} cells based on high expression of soluble enhanced yellow fluorescent protein (eYFP) in addition to the YFP–Cre fusion protein. **b**, YFP^{bright} T_{reg} from $F^{cre} \times C1^{+/+}$ or $F^{cre/+} \times C1^{f/+}$ or $C1^{f/f}$ mice and CellTrace Violet-labelled T_{conv} cells from $F^{cre} \times C1^{+/+}$ mice were co-cultured at indicated ratios for three days in the presence of anti-CD3 antibodies and T-cell-depleted splenocytes, and suppression measured as reduction of T_{conv} cell proliferation. **c**, T_{reg} cells of various genotypes and T_{conv} cells were co-adoptively transferred into Rag-deficient hosts and their respective frequency in peripheral blood was determined eight weeks later. **d**, $CD4^+YFP^+$ T_{reg} cells of indicated genotypes were cultured without exogenous IL-2 on anti-CD3/CD28-coated or uncoated plates for 6 or 18 h and examined for reactivity with annexin V and the viability dye ZombieRed. **e**, $CD4^+YFP^{bright}$ cells were sorted from LNs of one-year-old and $F^{cre/+} \times C1^{+/+}$ (or $C1^{f/+}$, $C1^{f/f}$) $\times$ $ROSA26\text{-}stop^{f/f\text{-}YFP}$ mice and subsequently stained for expression of FOXP3 protein to determine the frequency of $FOXP3^-$ exT_{reg} cells. $^*P < 0.05$, $^{**}P < 0.01$, $^{***}P < 0.001$, $^{****}P < 0.0001$ (two-way ANOVA with Sidak post hoc test in **b**, **c**; two-tailed Student's *t*-test in **d**).

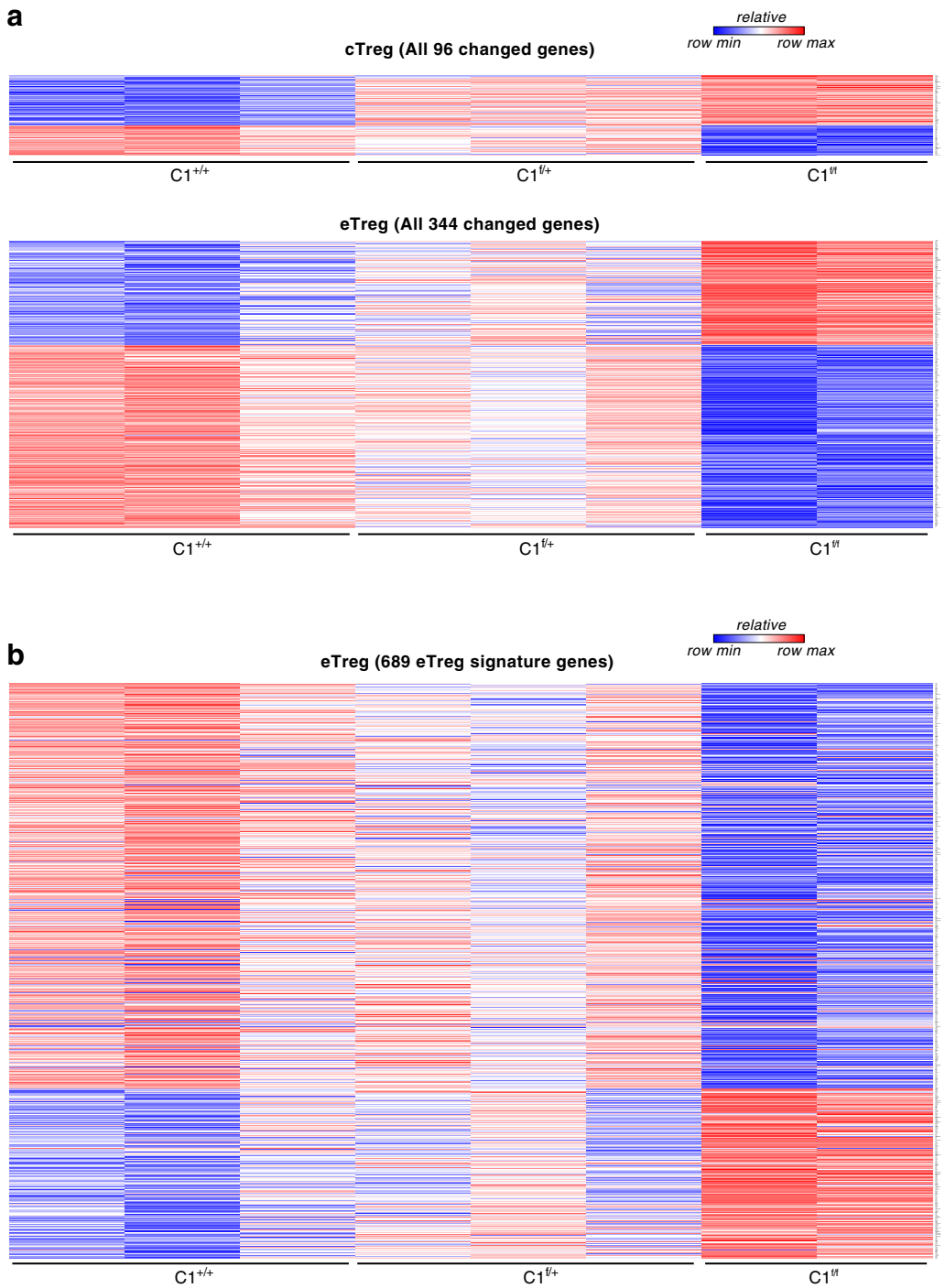

Extended Data Fig. 5 | Bulk RNA sequencing analysis of YFP$^+$ cT$_{reg}$ and eT$_{reg}$ cells from LNs of *F*$^{cre/+}$ × *C1*$^{+/+}$, *C1*$^{f/+}$ and *C1*$^{f/f}$ mice. **a**, Scaled expression in cT$_{reg}$ cells (top) and eT$_{reg}$ cells (bottom) of genes differentially expressed (fold change > 2 and $P_{adj} < 0.05$) between *C1*$^{+/+}$ and *C1*$^{f/f}$ mice. **b**, High-resolution, fully annotated heat map of eT$_{reg}$ signature genes as shown in Fig. 1j.

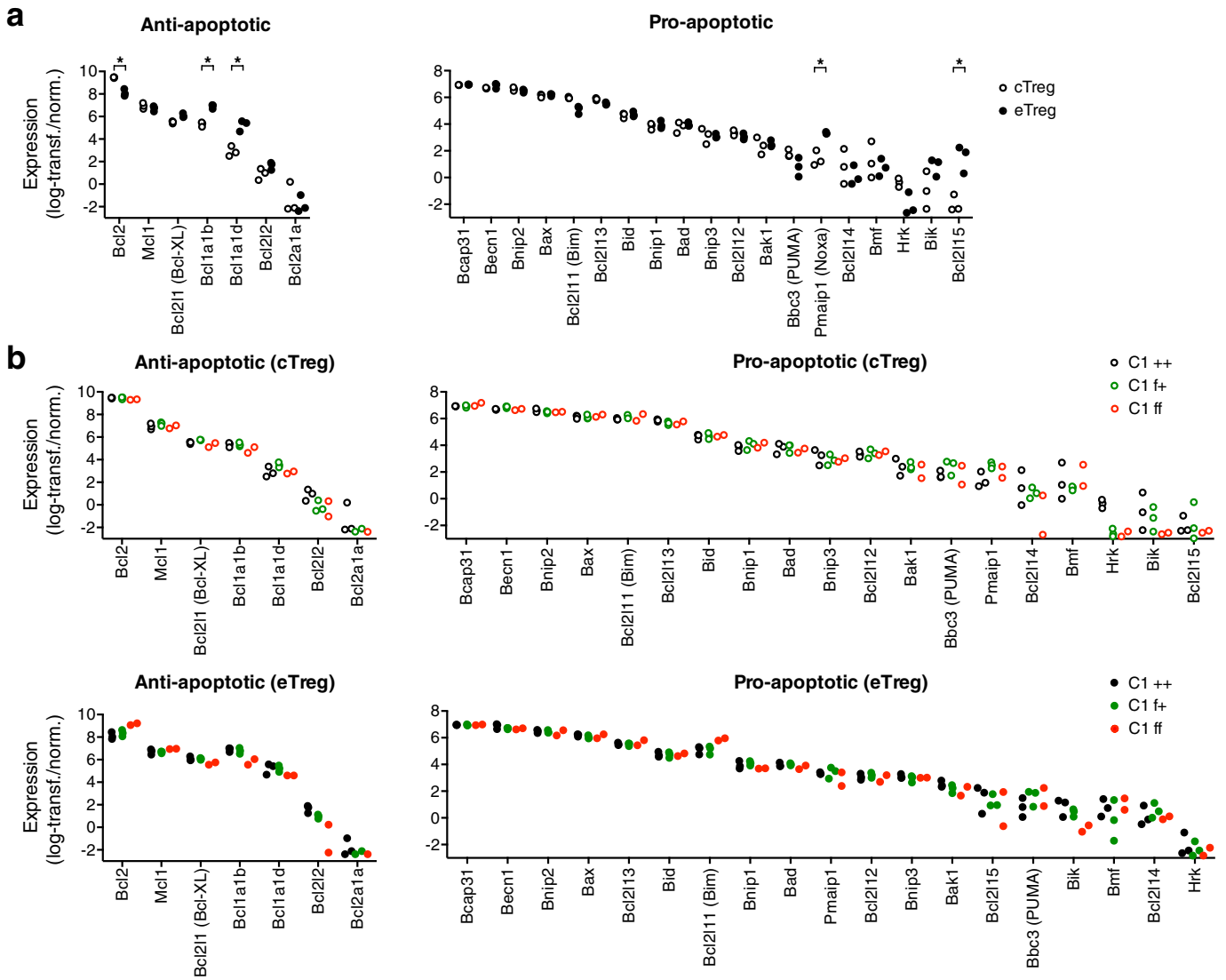

Extended Data Fig. 6 | Expression of apoptotic regulator genes. **a**, Comparison of normalized, log-transformed mRNA expression levels of anti- and pro-apoptotic Bcl2 family genes in YFP^+ cT_{reg} and eT_{reg} from $F^{cre/+} \times C1^{+/+}$ mice, based on RNA sequencing analyses. **b**, Comparison of expression of the same genes in cT_{reg} (top) and eT_{reg} (bottom) cells of the indicated genotypes. $*P_{adj} < 0.05$.

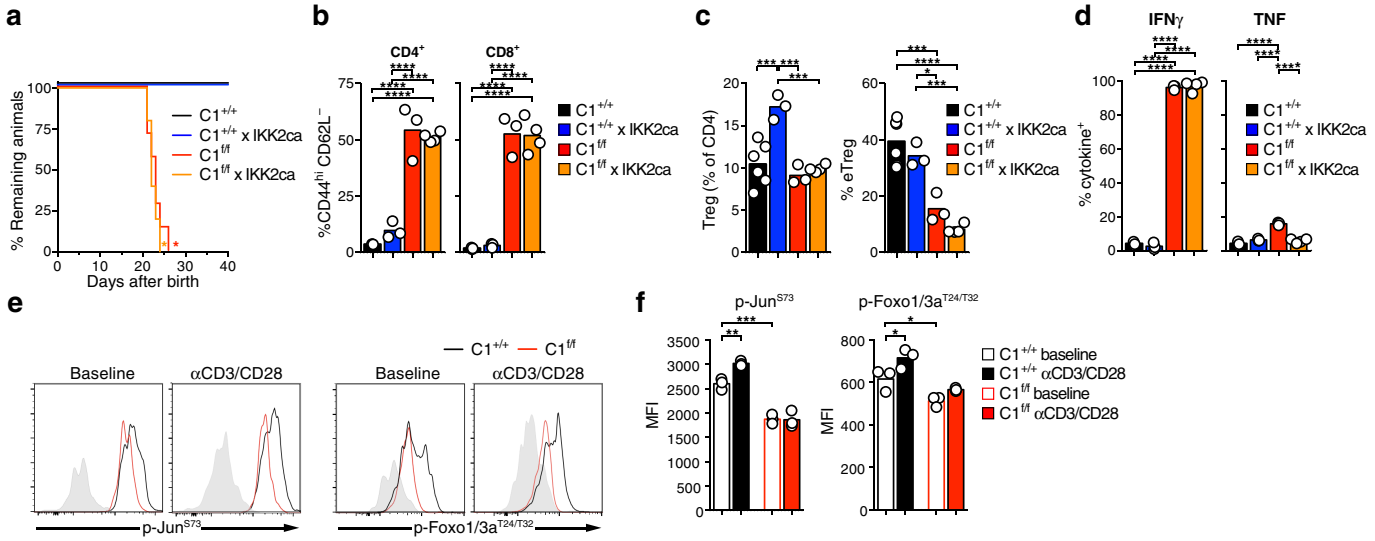

Extended Data Fig. 7 | Restoring NF-κB activation in CARMA1-deficient T_{reg} cells. a, Survival of $F^{cre} \times C1^{+/+}$ (or $C1^{f/f}$) × *ROSA26-stop*$^{f/f\text{-}IKK2ca}$ mice that express one allele of IKK2ca after expression of *Foxp3*^{cre}. **b**–**d**, Frequency of CD4$^+$ and CD8$^+$ T_{conv} cells with a CD44^{high} CD62L$^-$ effector memory phenotype in LNs (**b**), frequency of T_{reg} among CD4$^+$ T cells and of eT_{reg} cells among total T_{reg} cells in LNs (**c**), and effector cytokine expression of T_{conv} cells after 8-h ex vivo stimulation on anti-CD3/CD28-coated plates (**d**) in indicated mice. **e**, **f**, Expression of indicated phospho-proteins by YFP$^+$ T_{reg} cells from $F^{cre/+} \times C1^{+/+}$ or × $C1^{f/f}$ mice at baseline and after 30 min. Anti-CD3/CD28 in vitro stimulation. Grey solid histograms show unstained control cells. T_{conv} cells were used as internal controls, and showed no differences (not shown). $^*P < 0.05$, $^{***}P < 0.001$, $^{****}P < 0.0001$ (log-rank (Mantel–Cox) test in **a**; one-way ANOVA with Tukey post hoc test in **b**–**d**, **f**).

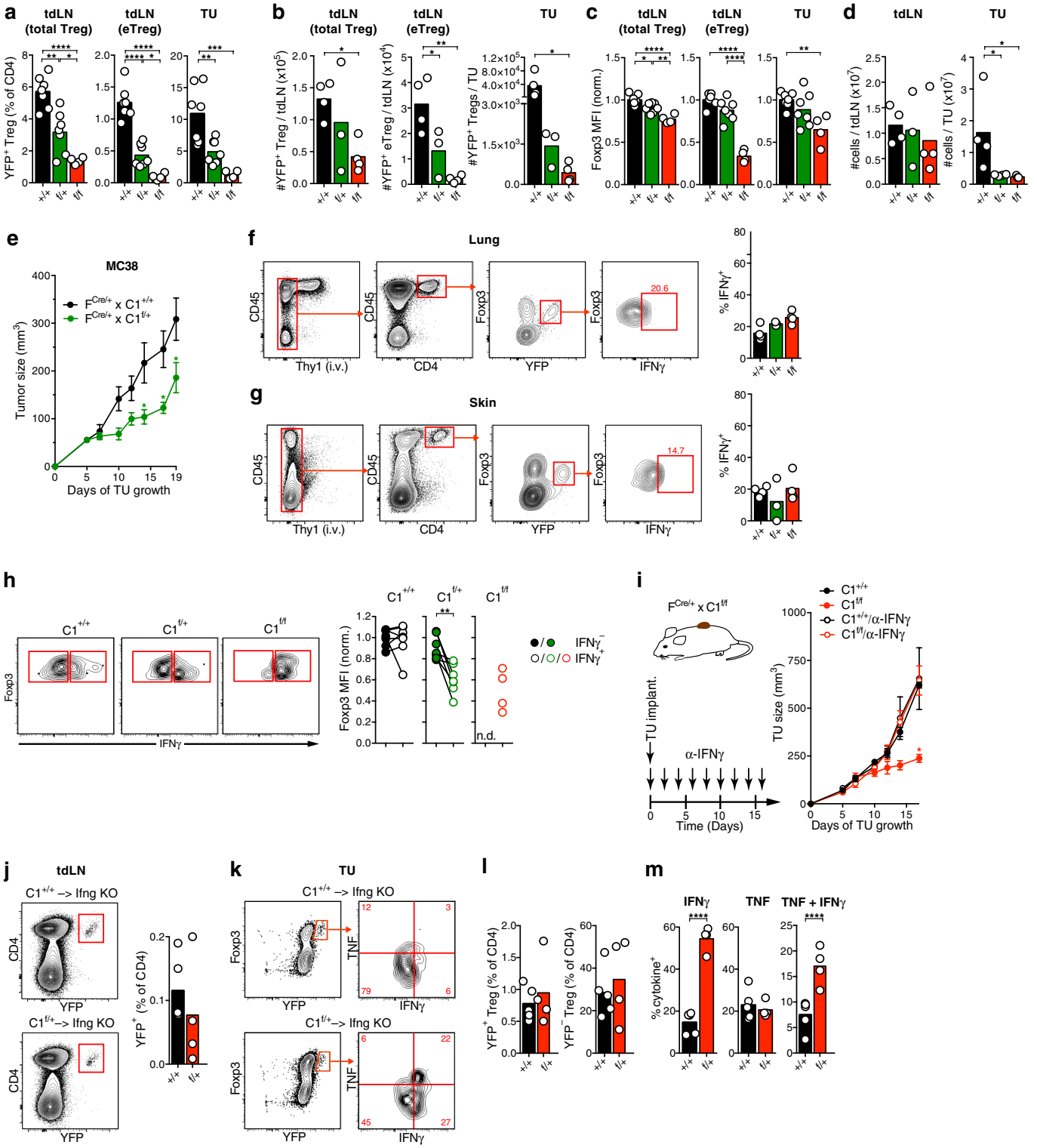

Extended Data Fig. 8 | Role of IFNγ secretion by FOXP3^{int} unstable T_{reg} cells selectively in tumour tissue. a–**c**, Frequencies of total YFP$^+$ T_{reg} cells and of YFP$^+$ eT_{reg} cells among CD4$^+$ T cells (**a**), absolute YFP$^+$ T_{reg} and eT_{reg} cell numbers (**b**), and normalized FOXP3 expression in YFP$^+$ T_{reg} and eT_{reg} (**c**) in tdLN and tumour tissue of 18-day-old D4M.3A tumours in female heterozygous $F^{cre/+} \times C1^{+/+}$, $C1^{f/+}$ or $C1^{f/f}$ mice. **d**, tdLN and tumour cellularities. **e**, Growth of MC38 tumours in female heterozygous $F^{cre/+} \times C1^{+/+}$ or $C1^{f/+}$ mice. **f**, **g**, Tumour-bearing mice were treated with brefeldin A for 5 h, injected intravenously with 3 μg of anti-THY1.2 monoclonal antibodies, and 3 min later collected for direct ex vivo analysis of IFNγ expression in extravascular YFP$^+$ T_{reg} cells in the lung (**f**) and skin (**g**). Gates for IFNγ$^+$ cells drawn based on fluorescence-minus-one (FMO) controls. **h**, Normalized FOXP3 expression in IFNγ$^+$ and IFNγ$^-$ T_{reg} cells from tumour tissue. n.d., not detectable. **i**, Tumour growth in indicated mice implanted with D4M.3A melanoma and19 treated with or without neutralizing anti-IFNγ antibody. **j**, Frequency of adoptively transferred, YFP$^+$ T_{reg} cells of indicated genotypes in tdLNs of *Ifng*$^{-/-}$ hosts at day 18 of tumour growth. **k**–**m**, Frequency (**k**, **l**) and effector cytokine expression (**m**) of adoptively transferred, YFP$^+$ T_{reg} cells in tumours in *Ifng*$^{-/-}$ hosts. $^*P < 0.05$, $^{**}P < 0.01$, $^{***}P < 0.001$, $^{****}P < 0.0001$ (one-way ANOVA with Tukey post hoc test in **a**–**d**, **f**, **g**; two-tailed Student's *t*-test in **e**, **h**, **j**, **l**, **m**; two-way ANOVA with Bonferroni post hoc test in **i**).

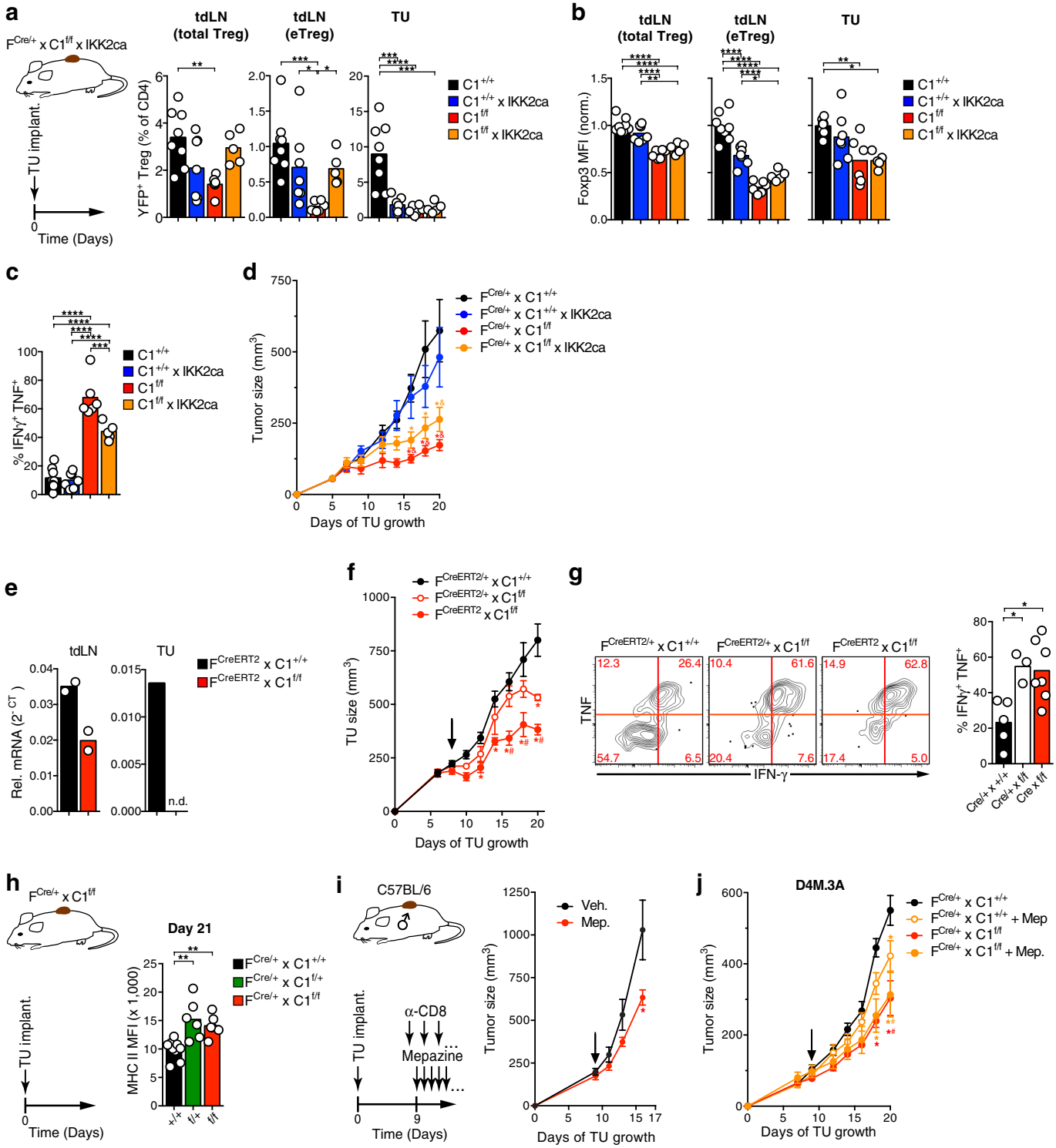

Extended Data Fig. 9 | Tumour response of CARMA1-deficient T_{reg} cells after restoration of NF-κB activation. a–d, D4M.3A melanoma cells were implanted into $F^{cre/+} \times C1^{+/+}$ (or $C1^{f/f}$) × $ROSA26\text{-}stop^{f/f\text{-}IKK2ca}$ mice to record frequencies of YFP^+ T_{reg} and eT_{reg} cells among $CD4^+$ T cells (**a**) and their normalized FOXP3 expression (**b**) in tdLNs and tumour tissue, effector cytokine expression by tumour-infiltrating T_{reg} cells (**c**), and tumour growth (**d**). **e**, YFP^+ T_{reg} cells were sorted from D4M.3A melanoma tissue and tdLNs after five days of treatment of $F^{creERT2} \times C1^{+/+}$ and $C1^{f/f}$ with tamoxifen and analysed for *CARMA1* expression by RT–qPCR. **f**, Tumour growth in female $F^{creERT2}$ or $F^{creERT2/+} \times C1^{+/+}$ and $C1^{f/f}$ mice, in which CARMA1 was deleted in all ($F^{creERT2}$) or half ($F^{creERT2/+}$) of T_{reg} cells. Arrow indicates tamoxifen treatment start. **g**, In situ expression in tumour tissue of effector cytokines by YFP^+ T_{reg} five days after CARMA1 deletion in half or all T_{reg} cells. **h**, MHC-II expression on tumour-associated macrophages in D4M.3A-implanted $F^{cre/+} \times C1^{+/+}$, $C1^{f/+}$ or $C1^{f/f}$ mice. **i**, D4M.3A tumour growth in mice treated with depleting anti-CD8 antibody from day 8 and treated with mepazine or vehicle from day 9. **j**, D4M.3A tumour growth in $F^{cre/+} \times C1^{+/+}$ or $C1^{f/f}$ mice treated with mepazine or vehicle starting on day 9. Data are mean and individual replicates or s.e.m. In **a**–**c**, **g**–**i**, $P < 0.05$, $^{**}P < 0.01$, $^{***}P < 0.001$, $^{****}P < 0.0001$. In **d**, $^{*}P < 0.05$ versus $C1^{+/+}$, &$P < 0.05$ versus $C1^{+/+}$ + IKK2ca. In **f**, $^{*}P < 0.05$ versus $F^{creERT2} \times C1^{+/+}$, #$P < 0.05$ versus $F^{creERT2/+} \times C1^{f/f}$. In **j**, $^{*}P < 0.05$ versus $C1^{+/+}$, #$P < 0.05$ versus $C1^{+/+}$ + mepazine (one-way ANOVA with Tukey post hoc test in **a**–**c**, **g**, **h**; two-way ANOVA with Bonferroni post hoc test in **d**, **f**, **j**: two-tailed Student's *t*-test in **i**).

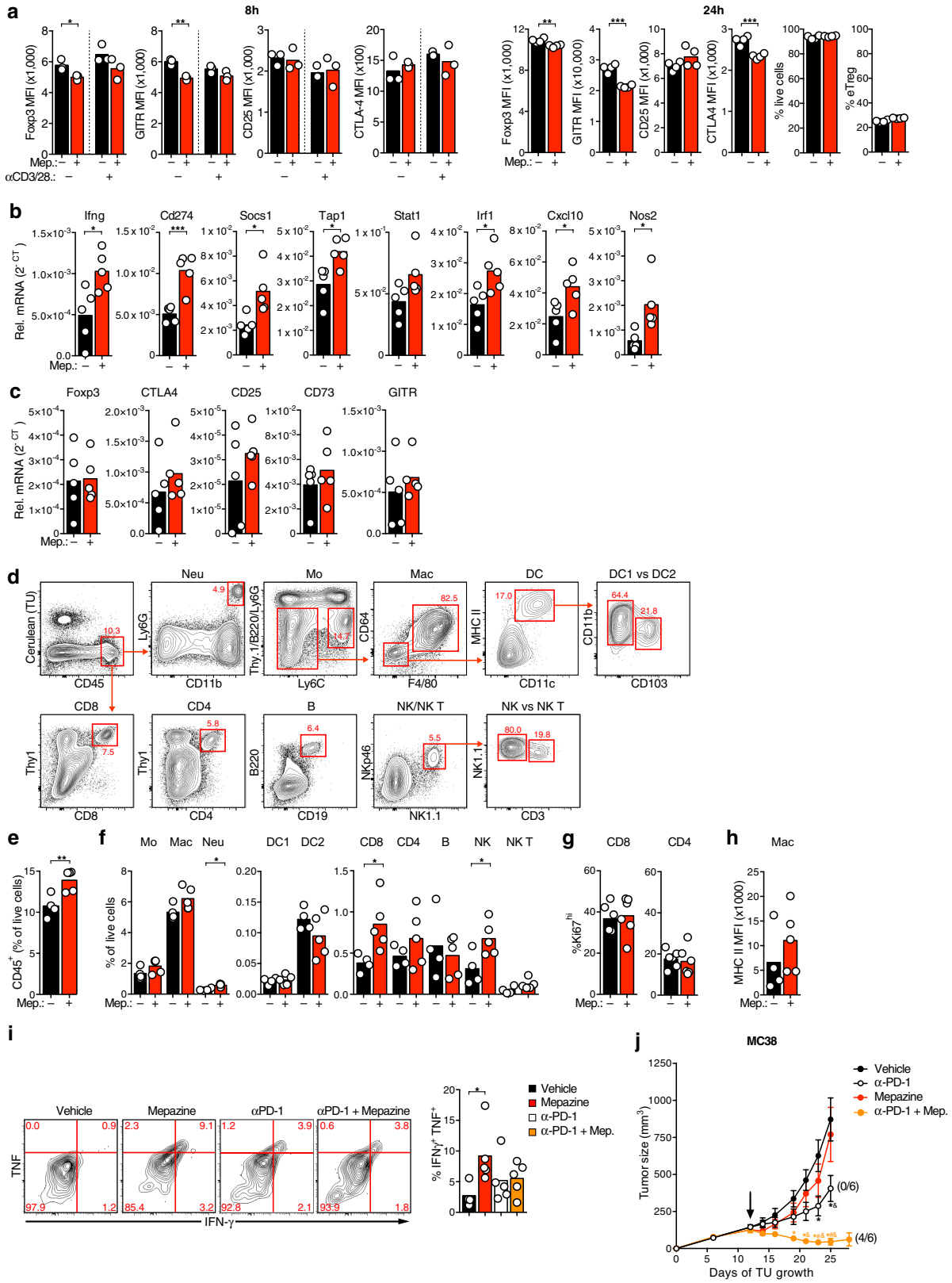

Extended Data Fig. 10 | See next page for caption.

Extended Data Fig. 10 | Mepazine effects on the tumour microenvironment. a, YFP^+ T_{reg} cells were sorted from $F^{cre} \times C1^{+/+}$ mice and treated with 10 μM mepazine or vehicle for 8 or 24 h with or without concurrent anti-CD3/28 monoclonal antibody TCR stimulation (8-h time point only). Expression of FOXP3, markers of eT_{reg} cell differentiation, cell viability, and frequency of eT_{reg} cells were recorded. **b**, **c**, RT–qPCR analysis of expression of *Ifng* and genes of adaptive immune resistance (the PD-L1 genes *Cd274* and *Socs1*), antigen presentation (*Tap1*), IFNγ signalling (*Stat1* and *Irf1*), T-cell recruitment (*Cxcl10*), M1 macrophage-activation (*Nos2*) (**b**) and of *Foxp3* and various T_{reg}-cell-associated genes (**c**) in whole tumour tissue lysate after three days of treatment with mepazine or vehicle control. **d**–**h**, Composition of the tumour tissue immune infiltrate and frequencies of $CD45^+$ cells (**e**) and of various immune cell subsets (**f**) as well Ki67 expression by T_{conv} cells (**g**) and MHC-II expression by macrophages (**h**) after three days of treatment with mepazine or vehicle control. **i**, Effector cytokine co-expression by tumour-infiltrating T_{reg} cells after 12 days of treatment with mepazine and anti-PD-1 antibody. **j**, Synergistic tumour control of MC38 colon carcinoma through anti-PD-1 and mepazine combination treatment in female C57BL/6 hosts. Numbers in parentheses indicate fraction of mice without relapse for more than 12 months after discontinuation of treatment. In **j**, $*P < 0.05$ versus vehicle, $\#P < 0.05$ versus anti-PD-1, and $\&P < 0.05$ versus mepazine. In all other panels, $*P < 0.05$, $**P < 0.01$, $***P < 0.001$ (two-tailed Student's *t*-test in **a**–**c**, **e**–**h**; one-way ANOVA with Tukey post hoc test in **i**; two-way ANOVA with Bonferroni post hoc test in **j**).

nature research

Corresponding author(s): Thorsten R. Mempel, Mauro Di Pilato

Last updated by author(s): Apr 1, 2019

Reporting Summary

Nature Research wishes to improve the reproducibility of the work that we publish. This form provides structure for consistency and transparency in reporting. For further information on Nature Research policies, see Authors & Referees and the Editorial Policy Checklist.

Statistics

For all statistical analyses, confirm that the following items are present in the figure legend, table legend, main text, or Methods section.

n/a	Confirmed	
☐	☒	The exact sample size (*n*) for each experimental group/condition, given as a discrete number and unit of measurement
☐	☒	A statement on whether measurements were taken from distinct samples or whether the same sample was measured repeatedly
☐	☒	The statistical test(s) used AND whether they are one- or two-sided *Only common tests should be described solely by name; describe more complex techniques in the Methods section.*
☒	☐	A description of all covariates tested
☐	☒	A description of any assumptions or corrections, such as tests of normality and adjustment for multiple comparisons
☐	☒	A full description of the statistical parameters including central tendency (e.g. means) or other basic estimates (e.g. regression coefficient) AND variation (e.g. standard deviation) or associated estimates of uncertainty (e.g. confidence intervals)
☒	☐	For null hypothesis testing, the test statistic (e.g. *F*, *t*, *r*) with confidence intervals, effect sizes, degrees of freedom and *P* value noted *Give P values as exact values whenever suitable.*
☒	☐	For Bayesian analysis, information on the choice of priors and Markov chain Monte Carlo settings
☒	☐	For hierarchical and complex designs, identification of the appropriate level for tests and full reporting of outcomes
☒	☐	Estimates of effect sizes (e.g. Cohen's *d*, Pearson's *r*), indicating how they were calculated

Our web collection on statistics for biologists contains articles on many of the points above.

Software and code

Policy information about availability of computer code

Data collection	BD FACSDiva software (version 8.0.2), Illumina bcl2fastq2 Illumina software (version 2.17.1.14), Zeiss Zen software 2010.
Data analysis	GraphPad Prism 6 FlowJo v9.9.5 and 10.5.3 Limma package in R.

For manuscripts utilizing custom algorithms or software that are central to the research but not yet described in published literature, software must be made available to editors/reviewers. We strongly encourage code deposition in a community repository (e.g. GitHub). See the Nature Research guidelines for submitting code & software for further information.

Data

Policy information about availability of data

All manuscripts must include a data availability statement. This statement should provide the following information, where applicable:

- Accession codes, unique identifiers, or web links for publicly available datasets
- A list of figures that have associated raw data
- A description of any restrictions on data availability

RNA-seq data will be deposited to the Gene Expression Omnibus (GEO). All other data of this study are available from the corresponding authors upon request.

Field-specific reporting

Please select the one below that is the best fit for your research. If you are not sure, read the appropriate sections before making your selection.

☒ Life sciences ☐ Behavioural & social sciences ☐ Ecological, evolutionary & environmental sciences

For a reference copy of the document with all sections, see nature.com/documents/nr-reporting-summary-flat.pdf

Life sciences study design

All studies must disclose on these points even when the disclosure is negative.

Sample size	No statistical methods were used to predetermine sample size, which were chosen based on prior experience with the same experimental design
Data exclusions	2 samples were excluded from RNA sequencing analysis due to contamination of the sorted cell population with irrelevant immune cells, as described in the methods section.
Replication	The experiments shown in Ext. Data Fig. 3b-c, 4a-e. 5a-b, 6a-b, 7a-h ,9a-c and k, and Fig. 1n-p and 4i-j have been performed once. All other experiments were repeated at least 2 or 3 times with similar results.
Randomization	Unless when restricted by genotype of the animals, mice were randomized into groups, e.g. for therapeutic tumor growth studies (e.g Mepazine and anti-PD1).
Blinding	For tumor growth assessments, the investigator was aware of host genotype and whether vehicle or drug was transferred into tumor-bearing mice.

Reporting for specific materials, systems and methods

We require information from authors about some types of materials, experimental systems and methods used in many studies. Here, indicate whether each material, system or method listed is relevant to your study. If you are not sure if a list item applies to your research, read the appropriate section before selecting a response.

Materials & experimental systems

n/a	Involved in the study
☐	☒ Antibodies
☐	☒ Eukaryotic cell lines
☒	☐ Palaeontology
☐	☒ Animals and other organisms
☒	☐ Human research participants
☒	☐ Clinical data

Methods

n/a	Involved in the study
☒	☐ ChIP-seq
☐	☒ Flow cytometry
☒	☐ MRI-based neuroimaging

Antibodies

Antibodies used

Antibody-Dye (Clone), Catalog-Number, Lot-Number, Supplier;
Anti-GFP-AlexaFluor488 (rabbit polyclonal), A21311, 1891008, Invitrogen;
Anti-Human/Mouse CARD11/CARMA1 (1D12), 04/2017, 5, Cell Signaling Technologies;
Anti-Human/Mouse/Rat Bim-PE (C34C5), 11/2017, 7, Cell Signaling Technologies;
Anti-Human/Mouse Phospho-c-JUN (Ser73) (D47G9) 11/2018, 3, Cell Signaling Technologies;
Anti-Mouse Phospho-FoxO1 (Thr24)/FoxO3a (Thr32), 11/2018, 7, Cell Signaling Technologies;
Anti-Mouse CD11b-PE/Cy7 (M1/70), 101216, B203625, BioLegend;
Anti-Mouse CD11b-FITC, (M1/70), 101215, B246149, BioLegend;
Anti-Mouse CD120b-Biotin (TR75-89), 113403, B200975, BioLegend;
Anti-Mouse CD152-APC (UC10-4B9), 106310, B230773, BioLegend;
Anti-Mouse CD152-BrilliantViolet605 (UC10-4B9), 106323, B233636, BioLegend;
Anti-Mouse CD274-PE (10F.9G2), 124307, B223286, BioLegend;
Anti-Mouse CD279 (29F.1A12), BE0273, 667617A2, BioXCell;
Anti-Mouse CD357-APC (DTA-1), 126312, B218262, BioLegend;
Anti-Mouse CD4-APC/Cy7 (GK1.5), 100414, B237980, BioLegend;
Anti-Mouse CD45-AlexaFluor700 (30-F11), 103128, B241345, BioLegend;
Anti-Mouse CD45- PerCP/Cy5.5 (30-F11), 103132, B249564, BioLegend
Anti-Mouse CD62L-BrilliantViolet421 (MEL-14), 104435, B238233, BioLegend;
Anti-Mouse CD62L-BrilliantViolet510 (MEL-14), 104441, B213054, BioLegend;
Anti-Mouse CD62L-PE/Cy7 (MEL-14), 104418, B209901, BioLegend;
Anti-Mouse CD73-AlexaFluor647 (TY/11.8), 127208, B228746, BioLegend;

Anti-Mouse CD8a-BrilliantViolet510 (53-6.7), 100751, B237067, BioLegend;
Anti-Mouse CD8a-PerCP/Cy5.5 (53-6.7), 100733, B249621, BioLegend
Anti-Mouse CD90.2-AlexaFluor700 (30-H12), 105320, B207170, BioLegend;
Anti-Mouse CD90.2-BrilliantViolet421 (30-H12), 105341, B240026, BioLegend;
Anti-Mouse CD90.2-PE/Cy7 (30-H12), 105325, B244113, BioLegend;
Anti-Mouse CD90.2-APC (30-H12), 105311, B244113, BioLegend;
Anti-Mouse CD90.2-Pacific Blue (53-2.1), 104306, B245912, BioLegend;
Anti-Mouse F4/80-APC (BM8), 123116, B241397, BioLegend;
Anti-Mouse F4/80-BrilliantViolet510 (BM8), 123135, B254669, Biolegned;
Anti-Mouse H-2Kb-PerCP/Cy5.5 (AF6-88.5), 116516, B188334, BioLegend;
Anti-Mouse I-A/I-E-BrilliantViolet605 (M5/114.15.2), 107639, B219482, BioLegend;
Anti-Mouse IFN-gamma (XMG1.2), BE0055, 630017J1, BioXCell;
Anti-Mouse IFN-gamma-AlexaFluor700 (XMG1.2), 505824, B224155, BioLegend;
Anti-Mouse IFN-gamma-PE (XMG1.2), 505808, B213720, BioLegend;
Anti-Mouse IFN-gamma-PE/Cy7 (XMG1.2), 505826, B217032, BioLegend;
Anti-Mouse IL-17A-PE/Cy7 (TC11-18H10.1), 506921, B236124, BioLegend;
Anti-Mouse IL-4-PerCP/Cy5.5 (11B11), 504123, B204723, BioLegend;
Anti-Mouse Ki67-BrilliantViolet605 (16A8), 652413, B223900, BioLegend;
Anti-Mouse Ki67-FITC (B56), 556026, 6312779, BD Biosciences;
Anti-Mouse Ly-6C-PerCP/Cy5.5 (HK1.4), 128012, B229409, BioLegend;
Anti-Mouse Ly-6C-APC/Cy7 (HK1.4), 128025, B2478350, Biolegend
Anti-Mouse TNF-AlexaFluor647 (MP6-XT22), 506314, B232130, BioLegend;
Anti-Mouse TNF-BrilliantViolet605 (MP6-XT22), 506329, B238894, BioLegend;
Anti-Mouse TruStain fcX (93), 101320, B234518, BioLegend;
Anti-Mouse/Human CD44-AlexaFluor700 (IM7), 103026, B244378, BioLegend;
Anti-Mouse/Human CD44-BrilliantViolet605 (IM7), 103047, B236770, BioLegend;
Anti-Mouse/Human CD44-PerCP/Cy5.5 (IM7), 103032, B213817, BioLegend;
Anti-Mouse/Rat Foxp3-AlexaFluor700 (FJK-16s), 56-5773-82, 4307313, eBioscience;
Anti-Mouse/Rat FoxP3-PE (FJK-16s), 12-5773-82, 4307350, eBioscience;
Anti-Mouse/Rat FoxP3-PE-Cy7 (FJK-16s), 25-5773-80, 4307350, eBioscience;
Anti-Rabbit Ig (H+L) goat-AlexaFluor488 (Polyclonal), A11008, 1583138, Life Technologies;
Anti-Rabbit Ig (H+L) goat-AlexaFluor405 (Polyclonal), A31556, 1984053, Life Technologies;
Rat IgG2a isotype control (2A3), BE0089, 654817O1, BioXCell;
Streptavidin-AlexaFluor700, S21383, 1800816, Invitrogen;
Streptavidin-PE/Cy7, 405206, B207311, BioLegend;
Zombie Red Fixable Viability Kit, 423110, 223441, BioLegend.
Anti-Mouse Tbet-BrilliantViolet 421 (4B10), 644815, B210885, BioLegend;
Anti-Mouse GATA3-PE-CF594 (L50-823), 563510, 7202530, BD Biosciences;
Anti-Human/Mouse ROR gamma (t)-PE (AFKJS-9), 12-6988-80, 4330086, Invitrogen;
Anti-mouse Ly-6G-APC (1A8), 127613, B259669, Biolegend;
Anti-mouse/human CD45R/B220-APC (RA3-6B2), 103212, B172317, BioLegend;
Anti-mouse Bcl-2 (BCL/10C4), 633510, B253631, Biolegend;
Anti-mouse CD64 (FcγRI)-PE (X54-5/7.1), 139303, B245515, Biolegend;
Anti-mouse CD11c-FITC (N418), 117305, B244373, BioLegend;
Anti-Mouse CD11c-PE/Cy7 (HL3), 561022, 7223543, eBioscience;
Anti-mouse CD103-PerCP/Cy5.5 (2E7), 121416, B252750, BioLegend;
Anti-mouse NK-1.1-PE/Cy7 (PK136), 108713, B249073, BioLegend;
Anti-mouse CD335 (NKp46)-APC (29A1.4), 137607, B252577, BioLegend;
Anti-mouse CD3-PerCP/Cy5.5 (17A2), 100217, B260626, BioLegend;
Anti-mouse CD25-PE-Cy7 (PC61.5), 25-0251-81, 4289561, eBioscience;
Anti-mouse CD19-PerCP/Cy5.5 (1D3/CD19) 152405, B255188 Biolegend;
Anti-mouse CD45RB-PE (16A), 553101, 7348606, BD Biosciences;
Anti-Mouse IgG (H+L)-Alexa Fluor647, A-21235,1764240, Thermo Fisher.

Validation

All antibodies are commercially available and validated by previous studies done by others or our laboratory.

Eukaryotic cell lines

Policy information about cell lines

Cell line source(s)

The BRAF^V600E x PTEN^null melanoma cell line, D4M.3A, was provided by David E. Fischer.
D4M.3A-H2B-Cerulean and D4M.3A-SIINFEKL-H2B-Cerulean were generated by the Mempel Laboratory through lentiviral transduction.
The colon adenocarcinoma cell line, MC38, was provided by Andrew D. Luster.

Authentication

D4M.3A cells were exome sequenced and determined to be of mouse origin.

Mycoplasma contamination

All cell lines were regularly tested for mycoplasma contamination.

Commonly misidentified lines
(See ICLAC register)

No cell line used is listed in the database of commonly misidentified cell lines maintained by ICLAC.

Animals and other organisms

Policy information about studies involving animals; ARRIVE guidelines recommended for reporting animal research

Laboratory animals	6 to 8 weeks old Foxp3^YFP-Cre, Foxp3^GFP-Cre-ERT2, Rosa26-STOP f/f-YFP, Rosa26-STOP f/f-IKK2ca, Ifng KO and C57BL/6J mice were purchased from Jackson Laboratories. Ramnik J. Xavier and James J. Moon (MGH) provided CARMA1^f/f and Rag1 KO mice, respectively. CARMA1^f/f mice were bred with Rosa26-STOP f/f-YFP, Rosa26-STOP f/f-IKK2ca and either Foxp3^YFP-Cre, Foxp3^GFP-Cre-ERT2, Rosa26^YFP.
Wild animals	No wild animals were employed in the study.
Field-collected samples	No field-collected samples were used in this study.
Ethics oversight	All mouse experiments were done with the approval of Institutional Animal Care and Use Committee.

Note that full information on the approval of the study protocol must also be provided in the manuscript.

Flow Cytometry

Plots

Confirm that:

☐ The axis labels state the marker and fluorochrome used (e.g. CD4-FITC).

☐ The axis scales are clearly visible. Include numbers along axes only for bottom left plot of group (a 'group' is an analysis of identical markers).

☒ All plots are contour plots with outliers or pseudocolor plots.

☒ A numerical value for number of cells or percentage (with statistics) is provided.

Methodology

Sample preparation	Heparinized peripheral blood collected through sub-mandibular vein puncture was treated with ACK red blood cell lysis buffer. LNs and spleens were passed through 40 um cell strainers, followed by red blood cell lysis (spleens only). Tumors and lungs were minced into small fragments and treated with 1.5 mg/ml collagenase IV and 50U/ml DNAse I for 30 min. at 37oC under agitation. Skin tissue was digested in medium containing 2% FCS, 10mM Hepes, 0.5 mg/ml hyaluronidase, 1.5 mg/ml collagenase IV, and 50 U/ml DNAse I for 45 min. at 37oC under agitation. Residual tissue fragments were mechanically dissociated. Cell surface proteins were stained for 20 minutes at 4oC. Intracellular and nuclear proteins were stained for 60 minutes at room temperature after permeabilization and fixation (Mouse regulatory T cell staining Kit; eBioscience). Preceding antibody staining, dead cells where stained using the fixable viability violet dye Zombie Red (Biolegend) for 15 minutes at room temperature, followed by blocking of Fc receptors with TruStain fcX (Biolegend) for 20 minutes at 4oC.
Instrument	Cells were analyzed on LSR II, LSRFortessa or LSRFortessa X-20 flow cytometers (BD Biosciences).
Software	BD FACSDiva was used to acquire the data. Data were analyzed with FlowJo software version 9.9.5 and 10.5.3.
Cell population abundance	10,000 CD4-pos. GFP-pos. cells from either lymph nodes or tumors of Foxp3^CreERT2 x CARMA1 +/+ or fl/fl mice were purified to >99% purity for RT-PCR analysis. 100,000 CD4-pos. YFP-pos. cells from lymph nodes of Foxp3^Cre/+ x CARMA1 +/+, or fl/fl x R26^YFP mice were purified to >99% purity for the in vitro apoptosis assay. 10,000 CD4-pos. YFP-pos. cells from lymph nodes of Foxp3^Cre/+ x CARMA1 +/+, fl/+, or fl/fl x R26^YFP mice were purified to >99% purity for Foxp3 staining. 5,000 CD4-pos. YFP-pos. CD44-low CD62L-pos cTreg/animal and the same number of CD4-pos. YFP-pos. CD44-high CD62-Lneg eTreg/animal from lymph nodes of Foxp3^Cre/+ x CARMA1 +/+, fl/+, or fl/fl x R26^YFP mice were purified to >99% purity for RNA-sequencing studies. 6,000,000 CD4-pos. CD45Rb-high YFP-neg. cells from lymph nodes of Foxp3^Cre/Cre x CARMA1 +/+ and 600,000 CD4-pos. YFP-pos. cells from lymph nodes of of Foxp3^Cre/+ x CARMA1 +/+, fl/+, or fl/fl x R26^YFP mice were purified to >98% purity for in vivo suppression study. 2,000,000 CD4-pos. YFP-neg. cells cells from lymph nodes of Foxp3^Cre/Cre x CARMA1 +/+ and 200,000 CD4-pos. YFP-pos. cells cells from lymph nodes of of Foxp3^Cre/+ x CARMA1 +/+, fl/+, or fl/fl x R26^YFP mice were purified to >98% purity for in vitro suppression study. CD4-pos. YFP-pos. cells from lymph nodes of of Foxp3^Cre/+ x CARMA1 +/+, fl/+ x R26^YFP mice were purified to >95% purity through magnetic-activated cell sorting (Miltenyi) purity and 1,000,000 cells/mouse injected for adoptive Treg cell transfer studies.
Gating strategy	Lymph node Treg analysis was gated on Zombie Red-negative, singlets, CD4-pos. CD8-neg./Foxp3-pos. events. Tumor Treg analysis was gated on Zombie Red-neg., CD45-pos. CD90-pos., singlets, CD4-pos. CD8-neg./Foxp3-pos. events. Tumor macrophage analysis was gated on Zombie Red-neg., CD45-pos., singlets, F4/80-pos. CD11b-pos. events. Tumor cell analysis was gated on Zombie Red-neg., CD45-neg., singlets, Cerulean-pos. events.

Splenic myeloid compartment was gated on CD11b-pos. and proportions of Ly6G-pos. neutrophils, CD11c-pos. MHC II-high DCs, Ly6C-high monocytes, Lyc6G-low SSC-high eosinophils, and Ly6C-low SSC-low macrophages were defined.
Tumor tissue immune infiltrates were gated on CD45pos. cells and proportion of CD90-pos. CD8-pos T cells, CD90-pos. CD4-pos T cells,
B220-pos. CD19-pos. B cells, Nkp46-pos. NK1.1-pos CD3-pos./neg. NK/NKT cells, Ly6G-pos. CD11b-pos. Neutrophils, CD90-neg B220-neg Ly6G-neg Ly6C-pos Monocytes and Ly6C-neg CD64-pos. F4/80 pos. Macrophages, and CD64-neg. F4/80 neg. MHC II high CD11c pos. Dendritic cells were defined.
For analysis of skin and lung Tregs, we excluded cells stained in vivo by i.v.-injected Thy1 Ab, then gated on CD45+ CD4+, Foxp3-YFP+ cells.

☒ Tick this box to confirm that a figure exemplifying the gating strategy is provided in the Supplementary Information.